S1P2, the G protein-coupled receptor for sphingosine-1- phosphate, negatively regulates tumor angiogenesis and tumor growth in vivo in mice

$S1P_2$, the G protein-coupled receptor for sphingosine-1-phosphate, negatively regulates tumor angiogenesis and tumor growth *in vivo* in mice

Wa Du[1], Noriko Takuwa[1,2], Kazuaki Yoshioka[1], Yasuo Okamoto[1], Koichi Gonda[3], Kazushi Sugihara[5], Akiyoshi Fukamizu[4], Masahide Asano[5] and Yoh Takuwa[1]

[1]Department of Physiology, Kanazawa University Graduate School of Medicine, Kanazawa, Japan; [2]Department of Health Science and Medicine, Ishikawa Prefectural Nursing University, Kahoku, Japan; [3]Department of Plastic Surgery, University of Tokyo Graduate School of Medicine, Tokyo, Japan; [4]Center for Tsukuba Advanced Research Alliance, Graduate School of Life and Environmental Sciences, University of Tsukuba, Tsukuba, Japan; [5]Division of Transgenic Animal Science, Advanced Science Research Center, Kanazawa University, Kanazawa, Japan

Financial support: This work was supported by grants from the Ministry of Education, Science, Sports and Culture of Japan and the Japan Society for the Promotion of Science.

Corresponding author: Yoh Takuwa, Department of Physiology, Kanazawa University Graduate School of Medicine, 13-1 Takara-machi, Kanazawa 920-8640, Japan.
Email:ytakuwa@med.kanazawa-u.ac.jp

Running title: **INHIBITION OF TUMOR ANGIOGENESIS BY $S1P_2$**

Key words: sphingosine-1-phosphate, S1P2, tumor angiogenesis, endothelial cells, myeloid cells

Abstract

Sphingosine-1-phosphate (S1P) has been implicated in tumor angiogenesis by acting via a G_i-coupled chemotactic receptor $S1P_1$. We report here that $S1P_2$, which, distinctly from $S1P_1$, mediates S1P inhibition of Rac and cell migration via $G_{12/13}$ and the Rho pathway, negatively regulates tumor angiogenesis and tumor growth. By using $S1P_2^{LacZ/+}$ mice, we found that $S1P_2$ was expressed in tumor vessels and normal blood vessels in many organs in both endothelial cells (ECs) and vascular smooth muscle cells, as well as tumor-associated, CD11b-positive bone marrow-derived cells (BMDCs). Lewis lung carcinoma (LLC) and B16BL6 melanoma tumors implanted in *S1P*$_2$-deficient ($S1P_2^{-/-}$) mice showed accelerated tumor growth and stimulated angiogenesis with enhanced association of vascular smooth muscle cells and pericytes. Compared with $S1P_2^{+/+}$ ECs, $S1P_2^{-/-}$ ECs showed enhanced Rac activity, Akt phosphorylation, cell migration, proliferation and tube formation *in vitro*. Co-injection of $S1P_2^{-/-}$ ECs and tumor cells into $S1P_2^{+/+}$ mice enhanced tumor growth and angiogenesis *in vivo*, as compared with co-injection of $S1P_2^{+/+}$ ECs and tumor cells. The recruitment of CD11b-positive BMDCs into tumors in $S1P_2^{-/-}$ mice was increased, compared with tumors in $S1P_2^{+/+}$ siblings. The bone marrow transplantation experiments showed that deletion of $S1P_2$ exclusively in BMDCs promoted tumor growth and angiogenesis. These results indicate that, in contrast to endothelial $S1P_1$ which stimulates tumor angiogenesis, $S1P_2$ on ECs and BMDCs mediates potent inhibition of tumor angiogenesis, providing a novel therapeutic strategy for anti-cancer treatment.

Introduction

Tumor growth critically depends upon neovascularization, in which endothelial cells (ECs) in preexisting blood vessels located in the vicinity of tumors are induced to migrate toward a tumor, proliferate and develop morphogenesis to form networks of microvessels in a tumor (1-3). Pericytes and vascular smooth muscle cells (VSMCs) are recruited to the newly formed microvessel wall to stabilize them (4-6), establishing functional tumor vessels that facilitate oxygen and nutrient supply for rapidly proliferating tumor cells. These processes are regulated by multiple extracellular signaling molecules including vascular endothelial growth factors (VEGFs), angiopoietin-1, fibroblast growth factors (FGFs) and platelet-derived growth factors (PDGFs), which are derived from both hypoxic tumor cells and infiltrating bone marrow-derived cells (BMDCs), the latter being also recruited by tumor itself (7-11). A subpopulation of BMDCs is also suggested to contribute to tumor angiogenesis through their differentiation into endothelial cells (12, 13).

Sphingosine-1-phosphate (S1P) is a pleiotropic lysophospholipid mediator that regulates cell proliferation, migration, survival, and differentiation by acting through members of the G protein-coupled S1P receptors, including widely expressed $S1P_1$, $S1P_2$ and $S1P_3$ (14). $S1P_1$, which is expressed on endothelial cells, mediates chemotaxis toward S1P and formation of capillary-like tube structures *in vitro* through mechanisms involving G_i-coupled activation of Rac small GTPase (15, 16). Deletion of *S1pr1* gene in mice resulted in embryonic lethality due to failure of vascular maturation (17, 18). RNAi-mediated $S1P_1$ silencing inhibited tumor angiogenesis and tumor growth *in vivo* in an animal model of subcutaneous tumor implantation (19), indicating that endogenous S1P is involved in tumor angiogenesis via $S1P_1$.

In sharp contrast to $S1P_1$, $S1P_2$ inhibits Rac and thereby cell migration via a $G_{12/13}$ /Rho-dependent mechanism (20, 21). $S1P_2$ is expressed at high levels in vascular smooth muscle cells (VSMCs) and certain types of tumor cells, mediating S1P inhibition of cell migration in these cell types (21-23). It was previously shown that deletion of $S1P_2$ leads to an age-dependent derangement in microvascular structure in the inner ear (24), and that deletion of $S1P_1$, $S1P_2$ and $S1P_3$ leads to a more severe phenotype regarding vascular maturation at the developmental stage compared with deletion of $S1P_1$ alone (25). We previously observed that endogenous $S1P_2$ mediated inhibition of Rac activity, cell migration and capillary-like tube formation in an endothelial cell line and that an $S1P_2$-selective antagonist enhanced *in vivo* angiogenesis in Matrigel plug assays (26). In addition, using both in vitro and in vivo models, several other groups have shown the anti-angiogenic activity of $S1P_2$ receptor (27, 28). However, it remains unknown whether and how $S1P_2$ is involved in tumor angiogenesis. The expression of $S1P_2$ *in vivo* in normal and tumor tissues has been little understood to date.

In the present study, by analyzing β-galactosidase (LacZ)-knockin mice in which LacZ gene expression is driven by endogenous $S1P_2$ promoter, we demonstrated for the first time that $S1P_2$ is expressed mainly in ECs and VSMCs of blood vessels in a variety of normal organs. In murine tumor isograft models, tumor vasculatures and infiltrating bone marrow-derived cells (BMDCs) expressed $S1P_2$. $S1P_2$-deficient ($S1P_2^{-/-}$) mice showed enhanced tumor angiogenesis and vascular maturation compared with wild-type ($S1P_2^{+/+}$) mice. Analysis of bone marrow-transplanted mice and the co-implantation experiments of isolated ECs and tumor cells provided evidence that $S1P_2$ in both ECs and BMDCs contributes to inhibition of tumor angiogenesis and tumor growth.

Materials and Methods

Tumor isograft models, Matrigel plug assay and bone marrow transplantation (BMT).

The conventional $S1P_2$-deficient mice and LacZ-knockin mice at the $S1P_2$ locus were generated as described in Supplementary Materials (Supplementary Figs. 1 and 2). Lewis lung carcinoma cells (LLC) (10^6) or B16BL6 (5×10^5) melanoma cells were injected into the right flanks of 8-week-old female $S1P_2^{+/+}$ and $S1P_2^{-/-}$ littermates (C57BL/6 background). In the co-implantation experiments, LLC or B16BL6 cells were mixed with $S1P_2^{+/+}$ or $S1P_2^{-/-}$ primary murine lung endothelial cells (MLECs, 2×10^5) and injected subcutaneously into wild-type mice. Tumor volume was determined every 2 days. Matrigel (300 μl, BD Biosciences) containing heparin (1 μg/ml, H3149, Sigma) with and without $VEGF_{165}$ and FGF2 (100 ng/ml each, PeproTech) were subcutaneously injected. In BMT experiments, the recipients were irradiated with a sublethal dosage of 9.6 Gy. Unfractionated bone marrow cells (10^7 cells) were collected by flushing the marrow cavity of femurs of $S1P_2^{+/+}$*;GFP* or $S1P_2^{Lacz/LacZ}$*;GFP* mice with PBS and injected into recipients via tail veins.

X-gal staining, immunohistochemistry, and immunofluorescence

Tumors or organs were snap-frozen in OCT compound. Cryosections (10 μm) were fixed and β-galactosidase activity was detected as blue pigments as described (29). Sections were counterstained with nuclear fast red (H-3403, Vector Laboratories).

For immunohistochemistry and immunofluorescence, cryosections were incubated with primary antibodies against CD31 (553171, clone MEC13.3, BD Biosciences),

von-Willebrand factor (vWF) (A0082, DAKO), CD11b (550282, BD Biosciences), Gr-1 (550291, BD Biosciences), desmin (M0760, clone D33, DAKO), NG2 (AB5320, Chemicon), phospho-Histone H3 (06-570, Upstate Biotechnology), and VE-cadherin (14-1441-81, eBioscinece), followed by incubation with the secondary antibodies conjugated with horse radish peroxidase, Alexa 594 or Alexa 488 and nuclear counterstaining with hematoxylin or DAPI (Molecular Probes). For determinations of functional microvessels with FITC-lectin staining, FITC-lectin (1mg/ml, FL-1171, Vector Laboratories) was injected into tail veins, followed by perfusion-fixation using 4% paraformaldehyde in Dulbecco's phosphate-buffered saline. The sections were observed with a microscope (Olympus, BX41) or confocal fluorescence microscope (Carl Zeiss LSM510 Pascal).

Preparation of primary mouse lung microvascular endothelial cells (MLECs) and determinations of cell proliferation, *in vitro* wound healing, and pull-down assay for GTP-bound Rac

MLECs were isolated from $S1P_2^{+/+}$ and $S1P_2^{-/-}$ mice with a magnetic separation method using a rat anti-mouse CD105 antibody (550546, BD Biosciences) and goat anti-rat antibody-conjugated magnetic beads, and MS columns (Miltenyi Biotec, Germany). All MLECs were cultured on plastic dishes coated with type I collagen (Nitta Gelatin), in EBM-2 medium (Lonza) containing growth factor supplements and 2% fetal bovine serum (FBS). MLECs showed purity greater than 95% by immunostaining with anti-CD31 and anti-VE-cadherin. For cell proliferation assay, the isolated MLECs were seeded onto 96 well plates the day before experiments, starved for 16 h in M199 medium containing 0.5% fatty acid free bovine serum albumin (BSA)

(Sigma), and transferred to EBM-2 containing 2% FBS, indicated concentrations of VEGF and Alamar Blue (BioSource, CA), followed by colorimetric measurements according to the manufacturer's instructions. For wound healing assay to evaluate cell migration, MLECs were seeded onto 60 mm dishes and allowed to grow until confluency. The cell monolayer was wounded with a plastic tip and cultured in EBM-2 media containing either 2% FBS and VEGF (100 ng/ml) or 10% FBS alone for indicated time periods. The pull-down assay for GTP-bound active Rac1 was performed as described in detail previously (20).

Bone marrow derived monocyte/macrophage (BMM) migration assay

BMMs (30) were used for transwell cell migration assay as described (20). Briefly, polycarbonate filters of 8μm pore size (Nucleopore, NeuroProbe) were coated with fibronectin (10μg/ml, Sigma). Dulbecco's modified Eagle's minimal essential medium (DMEM) with or without various amounts of MCP-1, VEGF or S1P was placed in the lower compartment of the chamber, and 5×10^5 cells/ml suspended in DMEM were added to the upper compartment. After incubation for 8 hours at 37 ℃, the number of cells that migrated through the filter was counted under a microscope.

Statistical analysis

Unless otherwise mentioned, the data are expressed as an average ±SEM. Two-way ANOVA was followed by Bonferroni's test to determine the statistical significance by using GraphPad Prism software. Unpaired Student's t-test was performed for the comparison between two groups. Error bars represent SEM for all figures. Statistical significance was defined as $*P<0.05$; $**P<0.01$; $***P<0.001$.

Results

LLC and B16BL6 melanoma cells were implanted into *S1P$_2^{-/-}$* and *S1P$_2^{+/+}$* littermate mice. For either LLC or B16BL6 the tumor volume was consistently larger in *S1P$_2^{-/-}$* mice than in wild-type mice, resulting in significant increases in the tumor weight in *S1P$_2^{-/-}$* mice at the end of experiments (Fig. 1A; supplementary Fig. 3A). Immunofluorescent staining of CD31 showed that the microvessel density (MVD) was greater in both LLC and B16BL6 tumors of *S1P$_2^{-/-}$* mice, compared with *S1P$_2^{+/+}$* littermates (Fig. 1B and C; Supplementary Fig. 3B and C). Consistently with increased MVD in tumors grown in *S1P$_2^{-/-}$* mice, the mRNA levels of CD31, VE-cadherin, VEGFR2 and Notch1, which are expressed in vascular ECs, were elevated in tumors of *S1P$_2^{-/-}$* mice (Supplementary Fig. 4). Probing with anti-phospho-histone H3 antibody revealed that the density of proliferating cell nuclei in LLC and B16BL6 tumors was greater in *S1P$_2^{-/-}$* compared with wild-type (Fig. 1B and C; Supplementary Fig. 3B and C). Most of anti-phospho-histone H3 positive proliferating cells were CD31-negative, suggesting that they were tumor cells. Proliferating cells were more abundantly observed in the areas of relatively high MVD in both *S1P$_2^{-/-}$* and *S1P$_2^{+/+}$* mice.

The extent of association of NG2-positive pericytes with CD31-positive microvessels in LLC tumors was more than two-fold increased in *S1P$_2^{-/-}$* mice compared with *S1P$_2^{+/+}$* mice (Fig. 2A). Similarly, the association with tumor microvessels of desmin-positive mural cells was greater in *S1P$_2^{-/-}$* compared with wild-type (Fig. 2B). The density of functional, perfused tumor microvessels was also more abundant in tumors grown in *S1P$_2^{-/-}$* mice than wild-type, as evaluated by intravenous injection of FITC-dextran followed by fluorescent microscopic observations of frozen tumor

sections (Supplementary Fig. 3D). Thus, tumors in *S1P$_2^{-/-}$* mice had increased numbers of more maturated, functional tumor microvessels.

In Matrigel plug assay, both *S1P$_2^{+/+}$* and *S1P$_2^{-/-}$* mice showed only moderate angiogenic activity of the similar extents in the absence of the growth factors as evaluated with anti-vWF staining of the Matrigel (Fig. 3A and B). In the growth factor-supplemented Matrigel, *S1P$_2^{-/-}$* mice showed a greater extent of stimulated neovessel formation with a 1.5-fold higher number of anti-vWF-positive cells compared with *S1P$_2^{+/+}$* mice. Immunohistochemistry using anti-desmin antibody, which stains both pericytes and VSMCs, showed a larger number of vascular mural cells in the Matrigel in *S1P$_2^{-/-}$* mice (Fig. 3C and D).

In normal tissues of *S1P$_2^{LacZ/+}$* mice, in which LacZ gene is knocked-in at the locus of *S1pr2* allele and LacZ expression is under the control of endogenous $S1P_2$ promoter, LacZ activity was detected with X-gal staining in various sizes of blood vessels in a variety of organs, which included lung, brain, skeletal muscle, kidney, and liver (Supplementary Fig. 5A). Vascular cells appeared to be the major cell types that expressed $S1P_2$ in many organs. Double staining with anti-CD31 and X-gal staining showed that ECs in microvessels and both ECs and VSMCs of larger vessels (for example, arteries in liver) expressed LacZ (Supplementary Fig. 5B). In addition, a limited population of bone marrow cells and non-vascular cells in the brain expressed LacZ (Supplementary Fig. 5A and B).

In LLC tumor isografts in *S1P$_2^{LacZ/+}$* mice, prominent LacZ expression was observed in hypervascular regions which were located at the tumor periphery, and blood vessels of a larger size in the adjacent peritumoral host tissue (Fig. 4A-a, b). The magnified views (Fig. 4A-c, d) revealed that LacZ-positive cells included microvascular

ECs in the tumor stroma and ECs and mural cells of a larger vessel in the peritumoral host tissue. Double staining with anti-CD31 immunohistochemistry and X-gal staining revealed that both ECs and mural cells of tumor vessels expressed LacZ (Fig. 4A-e, f). In addition, LacZ expression was detected in the scattered host-derived non-vascular cells both in the tumor stroma and in the tumor-surrounding host tissue (Fig. 4A-c, d). Compared with peripheral hypervascular regions, LacZ expressing cells were scanty in the central region of tumors (Fig. 4A-a).

More than 95% of MLEC monolayer cells isolated from $S1P_2^{+/+}$ and $S1P_2^{-/-}$ mice showed VE-cadherin assembly at the cell-cell boundary (Supplementary Fig. 6A). Essentially all of the MLECs cultured from $S1P_2^{LacZ/+}$ mice were positive for X-gal staining (Supplementary Fig. 6A), whereas MLECs from $S1P_2^{+/+}$ mice were negative, indicating that MLECs express $S1P_2$ in mice. The mRNA expression levels of $S1P_1$ or $S1P_3$ were not different between the ECs from $S1P_2^{+/+}$ and $S1P_2^{-/-}$ mice (Supplementary Fig. 7B). Immunofluorescence showed that $S1P_1$ expression in tumor blood vessels was similar between $S1P_2^{+/+}$ and $S1P_2^{-/-}$ mice (Supplementary Fig. 7A). MLECs derived from $S1P_2^{-/-}$ mice showed significantly higher rates of cell proliferation in response to serum with different concentrations of VEGF compared with $S1P_2^{+/+}$ mice (Fig. 4B). $S1P_2^{-/-}$ MLECs also showed augmented cell migration in *in vitro* wound healing assay in the presence of serum plus VEGF (Fig. 4C and Supplementary Fig. 6B) and serum alone (data not shown) as compared with $S1P_2^{+/+}$ MLECs. In *in vitro* tube formation assay, $S1P_2^{-/-}$ MLECs showed a higher morphogenic activity over $S1P_2^{+/+}$ MLECs in the presence of serum with or without VEGF, with respect to both the numbers of branching points and total length of tube-like structure (Supplementary Fig. 6C and D).

The basal Rac1 activity in unstimulated condition was approximately 1.6-fold

higher in $S1P_2^{-/-}$ MLECs compared with $S1P_2^{+/+}$ MLECs (Fig. 4D). Stimulation with VEGF or S1P resulted in Rac activation in both $S1P_2^{-/-}$ and $S1P_2^{+/+}$ MLECs over the respective basal levels, with greater extents of activation in $S1P_2^{-/-}$ MLECs; VEGF- and S1P-stimulated Rac1 activity in $S1P_2^{-/-}$ MLECs were higher by 1.5- and 2-fold, respectively, compared with $S1P_2^{+/+}$ MLECs. The total amounts of Rac1 protein were similar in $S1P_2^{+/+}$ and $S1P_2^{-/-}$ MLECs. Akt phosphorylation in response to S1P was different between $S1P_2^{+/+}$ and $S1P_2^{-/-}$ MLECs. In $S1P_2^{+/+}$ MLECs S1P rather reduced the extent of Akt phosphorylation, which was totally abolished in $S1P_2^{-/-}$ MLECs (Supplementary Fig. 8). The basal and VEGF-stimulated Akt phosphorylation was similar in both ECs. In contrast to Akt phosphorylation, the extents of ERK phosphorylation were not different between $S1P_2^{-/-}$ and $S1P_2^{+/+}$ MLECs under the basal or stimulated conditions.

We co-implanted tumor cells together with either $S1P_2^{-/-}$ or $S1P_2^{+/+}$ MLECs into wild type mice to evaluate the role of endothelial cell $S1P_2$ in the early phase of tumor growth and tumor angiogenesis. Tumor growth of either LLC or B16BL6 was accelerated when tumor cells were co-inoculated with $S1P_2^{-/-}$ MLECs compared with co-inoculation of tumor cells and $S1P_2^{+/+}$ MLECs (Fig. 5A and B, and Supplementary Fig. 9). Tumor microvessel density and FITC-lectin stained functional microvessel number in LLC tumors were significantly higher when co-injected with $S1P_2^{-/-}$ MLECs compared with $S1P_2^{+/+}$ MLECs (Fig. 5C and D).

Accumulated evidence shows that tumor infiltrating BMDCs, particularly $CD11b^+$ cells, are involved in tumor neovascularization through multiple mechanisms (31). We found that LLC tumors of $S1P_2^{-/-}$ mice showed a nearly 2-fold increase in the number of tumor infiltrating CD11b positive cells compared with $S1P_2^{+/+}$ mice (Fig. 6A, *upper*).

We explored the expression of $S1P_2$ in tumor-infiltrating bone marrow-derived cells (BMDCs) by inoculating LLC cells in $S1P_2^{+/+}$ mice that had received transplantation of bone marrow from $S1P_2^{LacZ/+}$ mice. LacZ-positive BMDCs were abundantly infiltrating into the tumor stroma in a scattered manner (Supplementary Fig. 10A). Double staining for LacZ activity and either of CD31, CD11b and Gr1 revealed that most, if not all, of LacZ-positive, infiltrating BMDCs were $CD11b^+Gr1^-CD31^-$ cells (Supplementary Fig. 10B-D). Immunohistochemistry of a pan-macrophage marker F4/80 showed that F4/80-positive macrophages were increased in tumors of $S1P_2^{-/-}$ mice compared with $S1P_2^{+/+}$ mice (Fig. 6A, *lower*). We studied motility of $CD11b^+$ bone marrow derived monocyte/macrophage (BMM). In a transwell migration assay, S1P in the lower chamber strongly inhibited migration toward VEGF of $S1P_2^{+/+}$-BMM, which was totally abolished in $S1P_2^{-/-}$-BMM (Fig. 6B). VEGFR1 mRNA expression was not different between $S1P_2^{+/+}$- and $S1P_2^{-/-}$-BMM (data not shown).

To address the role of $S1P_2$ expressed in BMDCs in tumor growth and neovessel formation, we inoculated LLC cells in $S1P_2^{+/+}$ mice that had undergone transplantation of bone marrow (BM) from either $S1P_2^{-/-}$ or $S1P_2^{+/+}$ donors. $S1P_2^{+/+}$ recipients reconstituted with $S1P_2^{-/-}$ BM cells showed significant stimulation of tumor volume and weight (Fig. 6C *upper*) and neovessel formation (Fig. 6D), compared with those reconstituted with $S1P_2^{+/+}$ BM cells. Conversely, $S1P_2^{-/-}$ recipients that had received $S1P_2^{+/+}$ marrow cells showed inhibition of tumor volume compared with those that had received $S1P_2^{-/-}$ marrow cells (Fig. 6C *lower*). We did not observe LacZ-positive cells in the vascular wall in LLC tumor in $S1P_2^{+/+}$ mice that had received transplantation of $S1P_2^{LacZ/+}$ BM (Supplementary Fig. 10B), suggesting that the contribution of $S1P_2$-expressing BMDCs as vascular cell precursors was minimal. In addition, the

mRNA levels of the angiogenic signaling molecules VEGF-A, TGFβ1, bFGF, and IL-1β among others were elevated in LLC tumors in *S1P$_2^{-/-}$* mice compared with wild-type (Supplementary Fig. 11).

Discussion

Accumulating evidence shows the emerging roles of the S1P signaling pathway in the regulation of blood vessel functions including vascular formation, vascular permeability, and the proliferative responses to injury (22, 32). Compared with $S1P_1$, the roles of $S1P_2$ in vascular pathophysiology are relatively poorly understood. In the present investigation, we studied the role of $S1P_2$ in tumor angiogenesis. The present study demonstrated that $S1P_2$ is expressed in both ECs and VSMCs of tumor blood vessels and BMDCs infiltrating in the tumor stroma, as well as in normal blood vessels in a variety of organs. Deletion of host $S1P_2$ resulted in stimulation of tumor angiogenesis with enhanced vascular mural cell recruitment and myeloid cell mobilization, leading to acceleration of tumor cell proliferation and tumor growth. These data collectively suggest that $S1P_2$, that is expressed in ECs and BDMC, is involved in suppression of tumor angiogenesis. The action of $S1P_2$ in tumor angiogenesis contrasts with $S1P_1$.

We found by the analysis of *S1P$_2^{LacZ/+}$* mice that vascular cells are the major cells that express $S1P_2$ in many organs. LacZ activity was particularly intense in pulmonary microvasculatures among other vascular beds (Supplementary Fig. 5A). Comparison of cultured lung ECs isolated from *S1P$_2^{+/+}$* and *S1P$_2^{-/-}$* mice demonstrated that Rac activity, cell proliferation, migration, and tube formation were enhanced in $S1P_2$-deficient MLECs *in vitro* (Fig. 4B-D, and Supplementary Fig. 6D). These observations, together

with the previous findings that $S1P_2$ is a negative regulator of Rac and cell migration (20, 33), suggested that deletion of $S1P_2$ induced de-inhibition of Rac activity in ECs, which, probably together with additional signaling pathways including PTEN downstream of $G_{12/13}$ and Rho, resulted in stimulation of cell migration and tube formation in $S1P_2^{-/-}$ MLECs. Furthermore, co-implantation studies of tumor cells and isolated MLECs (Fig. 5) provided evidence that deletion of endogenously expressed $S1P_2$ in ECs rendered them to become more potent in promoting tumor neovessel formation and tumor growth *in vivo* in an endothelial cell autonomous manner.

Increasing evidence shows that myeloid cells participate in tumor angiogenesis (31). In the present study, the bone marrow transplantation experiments revealed that $S1P_2$ expressed in BMDCs plays a significant role in the negative regulation of tumor neovascularization and tumor growth (Fig. 6C and D). We observed that $S1P_2$-expressing BMDCs include $CD11b^+Gr1^-$ myelomonocytic lineage cells (Supplementary Fig. 10C and D). Immunohistochemistry using anti-macrophage marker F4/80 showed that macrophages were more abundant in tumors of $S1P_2^{-/-}$ mice than of $S1P_2^{+/+}$ mice (Fig. 6A). Therefore, it is likely that at least a portion of $CD11b^+Gr1^-$ infiltrating cells represent macrophages.

These BMDCs were probably recruited by chemoattractants including chemokines, VEGF and other mediators that were secreted by tumor cells and tumor stroma cells. The migration study of isolated bone marrow-derived monocytes/macrophages showed that $S1P_2$ by itself was inhibitory for cell migration and exerted a strong inhibitory effect on VEGF-directed migration (Fig. 6B). The observations together with the increased infiltration of $CD11b^+$ and $F4/80^+$ myeloid cells in tumors of $S1P_2^{-/-}$ mice (Fig. 6A) suggest that $S1P_2$ exerts an inhibitory effect on recruitment of myeloid cells into

tumors. The infiltrating myeloid cells accumulating in tumors are known to release pro-angiogenic factors including VEGF, FGF2, PDGF and matrix metalloproteases (MMPs), the enzymes that contribute to angiogenesis through degradation of the extracellular matrix proteins and also release VEGF and TGFβ that had been deposited in the matrix (31, 34, 35). With this respect, we observed that tumors grown in $S1P_2^{-/-}$ mice showed increased mRNA expression levels of a panel of angiogenic molecules including VEGF and TGFβ. We also found an increased MMP9 activity in tumors of $S1P_2^{-/-}$ mice compared with $S1P_2^{+/+}$ mice by an in situ zymography technique, and increased VEGF mRNA expression in bone marrow-derived monocytes/macrophages from $S1P_2^{-/-}$ mice compared with $S1P_2^{+/+}$ mice (W. Du, unpublished observations). These observations suggest that more abundant BMDCs infiltrating in tumors of $S1P_2^{-/-}$ mice contribute to promotion of tumor growth at least in part through release of pro-angiogenic factors. Recent studies (35, 36) also suggested that a subpopulation of BMDCs is capable of transdifferentiating into vascular ECs and become incorporated into the new blood vessels in tumors. However, we could not detect LacZ-expressing bone marrow-derived ECs in tumor blood vessels in mice that underwent transplantation of $S1P_2^{LacZ/+}$ bone marrow.

In $S1P_2^{-/-}$ mice, the recruitment of mural cells to tumor blood vessels was promoted (Fig. 2). This may be explained by stimulated local production of angiogenic factors with a vascular maturation-promoting activity, which include TGFβ (Supplementary Fig. 11), the loss of chemorepulsion mediated by $S1P_2$ on mural precursor cells in the tumor microenvironment in which the concentration of S1P in the blood is presumed to be higher than in the perivascular tumor stroma, and the greater contribution of BMDCs as mural cell precursors (35, 36) in $S1P_2^{-/-}$ mice. Concerning the latter possibility,

LacZ-expressing mural cells were not readily detected in the vascular wall in tumors of mice that had received transplantation of $S1P_2^{LacZ/+}$ BM (Supplementary Fig. 10), suggesting that the incorporation of bone-marrow-derived mural cell precursors into the vascular wall was unlikely.

Recent studies showed that inhibition of $S1P_1$ action by either siRNA-mediated silencing (19) or functional downregulation of $S1P_1$ by the S1P analogue FTY720 phosphate inhibited tumor angiogenesis and tumor growth, suggesting the possibility that $S1P_1$ could be a target for ani-angiogenic therapy (37-39). Our observations that tumor neovessels, especially those in peripheral angiogenic hot spot regions, abundantly express $S1P_2$ (Fig. 4) strongly suggest the possibility that selective activation of $S1P_2$ may lead to inhibition of tumor angiogenesis and thus tumor growth. $S1P_1$ was shown to be upregulated in tumor blood vessels (19). It remains to be defined how the expression of $S1P_2$ is regulated in tumor vasculatures. It is an interesting possibility that S1P receptor subtype-selective pharmacological targeting strategies, i.e. $S1P_1$ inhibition in combination with $S1P_2$ activation, could lead to more effective inhibition of tumor angiogenesis. In addition to an expected anti-angiogenic action of $S1P_2$-selective agonist, which is mediated through $S1P_2$ expressed on ECs and BMDCs, selective activation of $S1P_2$ expressed on tumor cells is expected to directly inhibit tumor cell migration *in vivo*, leading to inhibition of invasion and metastasis, as we previously demonstrated in an animal model (40).

In conclusion, the present study demonstrated the novel inhibitory role of the S1P signaling pathway via $S1P_2$ in tumor angiogenesis. The $S1P_2$ effects involve EC-autonomous actions and myeloid cell-dependent actions. These observations open the possibility of a novel anti-angiogenic therapy to target $S1P_2$.

Acknowledgments

We thank K. Saikawa for helpful advice on histological preparations, Drs. Xuzhang Lu and Yu Wu for assistance with FACS and bone marrow transplantation. We thank Dr. M.Okabe for generous gift of GFP mice.

References:

1. Folkman J. The role of angiogenesis in tumor growth. Semin cancer Bio. 1992; 3: 65-71.

2. Risau W. Mechanisms of angiogenesis. Nature. 1997; 386: 671-4.

3. Coultas L, Chawengsaksophak K, Rossant J. Endothelial cells and VEGF in vascular development. Nature. 2005; 438: 937-45.

4. Gerhardt H, Betsholtz C. Endothelial-pericyte interactions in angiogenesis. Cell Tissue Res. 2003; 314: 15-23.

5. Darland DC, D'Amore PA. Cell-cell interactions in vascular development. Curr Top Dev Biol. 2001; 52: 107-49.

6. Armulik A, Abramsson A, Betsholtz C. Endothelial/pericyte interactions. Circ Res 2005; 97: 512-23.

7. Gerber HP, Kowalski J, Sherman D, et al. Complete inhibition of rhabdomyosarcoma xenograft growth and neovascularization requires blockade of both tumor and host vascular endothelial growth factor. Cancer Res. 2000; 60: 6253-8.

8. Stratmann A, Risau W, Plate KH. Cell specific expression of angiopoietin-1 and angiopoietin-2 suggests a role in glioblastoma angiogenesis. Am J Pathol. 1998; 153 1459-66.

9. Czubayko F, Liaudet-Coopman ED, Aigner A, et al. A secreted FGF-binding protein can serve as the angiogenic switch in human cancer. Nat Med. 1997; 3: 1137-40.

10. Lindblom P, Gerhardt H, Liebner S, et al. Endothelial PDGF-B is required for proper investment of pericytes in the microvessel wall. Genes Dev. 2003; 17: 1835-40.

11. Seandel M, Butler J, Lyden D, et al. A catalytic role for proangiogenic marrow-derived cells in tumor neovascularization. Cancer cell. 2008; 13: 181-3.

12. Gao D, Nolan DJ, Mellick AS, et al. Endothelial progenitor cells control the angiogenic switch in mouse lung metastasis. Science. 2008; 319: 195-8.

13. Lyden D, Hattori K, Dias S, et al. Impaired recruitment of bone-marrow-derived endothelial and hematopoietic precursor cells blocks tumor angiogenesis and growth. Nat Med. 2001; 7: 1194-201.

14. Ishii I, Fukushima N, Ye X, et al. Lysophospholipid receptors: signaling and biology. Annu Rev Biochem. 2004; 73: 321-54.

15. Lee MJ, Thangada S, Claffey KP, et al. Vascular endothelial cell adherens junction assembly and morphogenesis induced by sphingosine-1-phosphate. Cell 1999; 99: 301–12.

16. Ryu Y, Takuwa N, Sugimoto N, et al. Sphingosine-1-phosphate, a platelet-derived lysophospholipid mediator, negatively regulates cellular Rac activity and cell migration in vascular smooth muscle cells. Circ Res. 2002; 90: 325-32.

17. Liu Y, Wada R, Yamashita T, et al. Edg-1, the G protein-coupled receptor for sphingosine-1-phosphate, is essential for vascular maturation. J Clin Invest. 2000; 106 (8): 951-61.

18. Allende ML, Yamashita T, Proia RL. G-protein-coupled receptor S1P1 acts within endothelial cells to regulate vascular maturation. Blood. 2003; 102: 3665-7.

19. Chae SS, Paik JH, Furneaux H, et al. Requirement for sphingosine 1-phosphate receptor-1 in tumor angiogenesis demonstrated by in vivo RNA interference. J Clin Invest. 2004; 114: 1082-9.

20. Sugimoto N, Takuwa N, Okamoto H, et al. Inhibitory and stimulatory regulation of Rac and cell motility by the G12/13-Rho and Gi pathways integrated downstream of a single G protein-coupled sphingosine-1-phosphate receptor isoform. Mol Cell Biol.

2003; 23: 1534-45.

21. Takashima S, Sugimoto N, Takuwa N, et al. G12/13 and Gq mediate S1P2-induced inhibition of Rac and migration in vascular smooth muscle in a manner dependent on Rho but not Rho kinase. Cardiovasc Res. 2008; 79: 689-97.

22. Skoura A, Hla T. Regulation of vascular physiology and pathology by the S1P2 receptor subtype. Cardiovasc Res. 2009; 82: 221-8.

23. Lepley D, Paik JH, Hla T, et al. The G protein-coupled receptor S1P2 regulates Rho/Rho kinase pathway to inhibit tumor cell migration. Cancer Res. 2005; 65: 3788-95.

24. Kono M, Belyantseva IA, Skoura A, et al. Deafness and stria vascularis defects in S1P2 receptor-null mice. J Biol Chem. 2007; 282: 10690-6.

25. Kono M, Mi Y, Liu Y, et al. The sphingosine-1-phosphate receptors S1P1, S1P2, and S1P3 function coordinately during embryonic angiogenesis. J Biol Chem. 2004; 279: 29367-73.

26. Inoki I, Takuwa N, Sugimoto N, et al. Negative regulation of endothelial morphogenesis and angiogenesis by S1P2 receptor. Biochem Biophys Res Commun. 2006; 346: 293-300.

27. Skoura A, Sanchez T, Claffey K, et al. Essential role of sphingosine 1-phosphate receptor 2 in pathological angiogenesis of the mouse retina. J Clin Invest. 2007; 117: 2506-16.

28. Estrada R, Zeng Q, Lu H, et al. Up-regulating sphingosine-1-phosphate receptor-2 signaling impairs chemotactic, wound-healing, and morphogenetic responses in senescent endothelial cells. J Biol Chem. 2008; 283(44): 30363-75.

29. Seymour PA, Sander M. Immunohistochemical detection of beta-galactosidase or

green fluorescent protein on tissue sections. Methods Mol Biol. 2007; 411: 13-23.

30. Ryu J, Kim HJ, Chang EJ, et al. Sphingosine 1-phosphate as a regulator of osteocalst differentiation and osteoclast-osteoblast coupling. EMBO J. 2006; 25 (24): 5840-51.

31. Murdoch C, Muthana M, Coffelt SB, et al. The role of myeloid cells in the promotion of tumour angiogenesis. Nat Rev Cancer. 2008; 8: 618-631.

32. Takuwa Y, OkamotoY, Yoshioka K, et al. Sphingosine-1-phosphate signaling and biological activities in the cardiovascular system. Biochim Biophys Acta. 2008; 1781: 483-8.

33. Ryu Y, Takuwa N, Sugimoto N, et al. Sphingosine-1-phosphate, a platelet-derived lysophospholipid mediator, negatively regulates cellular Rac activity and cell migration in vascular smooth muscle cells. Circ Res. 2002; 90: 325-32.

34. Grunewald M, Avraham I, Dor Y, et al. VEGF-induced adult neovascularization: recruitment, retention, and role of accessory cells. Cell. 2006; 124: 175-89.

35. Shojaei F, Zhong C, Wu X, et al. Role of myeloid cells in tumor angiogenesis and growth. Trends Cell Bio. 2008; 18: 372-8.

36. Rajantie I, Ilmonen M, Alminaite A, et al. Adult bone marrow-derived cells recruited during angiogenesis comprise precursors for periendothelial vascular mural cells. Blood. 2004; 104: 2084-6.

37. LaMontagne K, Littlewood-Evans A, Schnell C, et al. Antagonism of sphingosine-1-phosphate receptors by FTY720 inhibits angiogenesis and tumor vascularization. Cancer Res. 2006; 66: 221-31.

38. Schmid G, Guba M, Ischenko I, et al. The immunosuppressant FTY720 inhibits tumor angiogenesis via the sphingosine 1-phosphate receptor 1. J Cell Biochem. 2007;

101: 259-70.

39. van Meeteren LA, Brinkmann V, Saulnier-Blache JS, et al. Anticancer activity of FTY720: phosphorylated FTY720 inhibits autotaxin, a metastasis-enhancing and angiogenic lysophospholipase D. Cancer Lett. 2008; 266: 203-8.

40. Yamaguchi H, Kitayama J, Takuwa N, et al. Sphingosine-1-phosphate receptor subtype-specific positive and negative regulation of Rac and haematogenous metastasis of melanoma cells. Biochem J. 2003; 374: 715-22.

Figure Legends

Figure 1. Enhanced tumor growth and angiogenesis of LLC in $S1P_2$ deficient mice. (A) Tumor volumes (*left*) and weights (*right*) of LLC inoculated subcutaneously in $S1P_2^{+/+}$ (solid lines) and $S1P_2^{-/-}$ (dotted lines) littermate mice were measured (n=14). (B) Representative images of LLC tumor blood vessel (*left*) and proliferating cell nuclei (*middle*) which were detected by anti-CD31 (red) and a mitotic marker, anti-phospho-Histone H3 (green) immunofluorescence, respectively. Tumors from $S1P_2^{-/-}$ hosts show increased vascularity and enhanced tumor cell proliferation. Scale bar=100 μm. (C) Numbers of tumor microvessels (*left*) and proliferating cell nuclei (*right*) in LLC tumors (n=9).

Figure 2. Tumor microvessels in $S1P_2$ deficient mice show increased mural cell recruitment. (A) and (B), the pericyte marker NG2 (A) and both pericyte and smooth muscle marker desmin (B) were detected by immunofluorescence (green) in LLC tumors grown in $S1P_2^{+/+}$ and $S1P_2^{-/-}$ mice. Representative images of double immunofluorescence for CD31 (red) and either of the mural cell markers are shown. The ratios in pixels of NG2 (A) and desmin (B) over CD31 were quantified by Image J software (*right*). (n=9).

Figure 3. $S1P_2$ deficient mice show enhanced angiogenesis with stimulated mural cell recruitment in endothelial growth factor-containing Matrigel Plugs. (A) The plugs that were either supplemented with VEGF (200 ng/ml) and FGF2 (100 ng/ml) or growth factor-deficient (PBS), were excised 10 days after implantation. The sections of Matrigel plugs obtained from $S1P_2^{+/+}$ and $S1P_2^{-/-}$ mice were immunostained with

anti-von Willebrand factor (vWF) antibody. Representative images are shown. (B) The numbers of vWF positive cells were quantified. (C) Representative images of immunostaining against desmin. *Arrow heads*, desmin positive cells. Scale bars (A and C):100 μm. (D) The quantified data of anti-desmin staining. In (B) and (D), the numbers of vWF positive cells and desmin positive cells per high power field (HPF) were quantified in $S1P_2^{+/+}$ and $S1P_2^{-/-}$ plug sections. (n=4).

Figure 4. Expression of $S1P_2$ in tumor vasculatures, and cell proliferation, migration, and Rac pull-down assay *in vitro* in $S1P_2$ deficient mouse lung endothelial cells (MLECs). (A) X–gal staining and CD31 immunostaining of serial sections of a LLC tumor at 14 days in $S1P_2^{LacZ/+}$ mice. *a* and *b*, X-gal staining positive cells were especially rich in peripheral hypervascular hot spot regions (*a*) where CD31 is strongly positive (*b*, yellow dash). Scale bar=500 μm. The magnified views of two *boxed areas* in *a* are shown in *c* and *d*. *c*, X-gal staining positive host cells are localized in both vessel walls and outside of vessels in the peri-tumoral region. T, tumor. *d*, X-gal staining-positive cells on the vascular wall (*black arrows*) and scattered cells in the tumor stroma outside of vessels (*orange arrows*). Scale bar=50 μm. *e* and *f*, double staining for X-gal and CD31 of tumor sections showing that $S1P_2$ is expressed in both endothelial and mural cells of tumor vessels. Scale bar=20 μm. (B) $S1P_2^{-/-}$ MLECs showed significantly higher rate of cell proliferation and saturation density compared with $S1P_2^{+/+}$ MLECs in the presence of indicated concentrations of VEGF. (C) *In vitro* wound healing assay of MLECs. $S1P_2^{-/-}$ MLECs showed significantly stimulated cell migration in the presence of serum and VEGF alone after 24 and 48 hours compared with $S1P_2^{+/+}$ MLECs. (D) Rac pull-down assay of $S1P_2^{+/+}$ and $S1P_2^{-/-}$ MLECs

stimulated with S1P (10^{-7} M) or VEGF(100 ng/ml) for 5 min.

Figure 5. $S1P_2$ deficient MLECs co-injected with tumor cells promote tumor growth and angiogenesis *in vivo*. (A) Representative images of LLC tumors, which had been implanted together with either $S1P_2^{+/+}$ or $S1P_2^{-/-}$ MLECs. (B) Growth curves of LLC tumors which were co-implanted with either $S1P_2^{+/+}$ or $S1P_2^{-/-}$ MLECs. (C) Tumor vessels in LLC co-implanted with either $S1P_2^{+/+}$ or $S1P_2^{-/-}$ MLECs were visualized by anti-CD31 immunostaining (*left*). Scale bar=100 μm. (D) FITC-lectin (1mg/ml) were i.v. injected into mice, and 3 min later mice were perfusion-fixed. The cryosections were immuno-stained with anti-CD31 antibody and observed under a fluorescent microscope. FITC-lectin labeled perfused microvessels and CD31-stained microvessels were counted per field. The ratio of FITC-lectin labeled microvessel number to CD31-positive microvessel number is shown in the bar graph (*right*). Scale bar=50 μm.

Figure 6. Deletion of $S1P_2$ in BMDCs promote tumor growth and tumor angiogenesis in $S1P_2^{+/+}$ mice. (A) $CD11b^+$ myeloid cell recruitment into tumors is promoted in $S1P_2^{-/-}$ mice. Sections of LLC tumors in $S1P^{+/+}$ and $S1P2^{-/-}$ mice were immunostained with anti-CD11b antibody, and $CD11b^+$ myeloid cells were counted. (B) Transwell migration of bone marrow derived monocyte/macrophage (BMM) from $S1P_2^{+/+}$ and $S1P_2^{-/-}$ mice. DMEM with 0.1% fatty acid free BSA (vehicle); MCP-1 (10ng/ml); VEGF (100ng/ml); S1P (10^{-7}M); were added to the lower compartment. Migrated cells in each microscopic field were counted. (C) LLC tumor growth curves and tumor weight for $S1P_2^{+/+}$ (*left*) and $S1P_2^{-/-}$ (*right*) mice that had received

transplantation of BM from either $S1P_2^{+/+}$ (solid line) or $S1P_2^{-/-}$ (dashed line) donors 5 weeks prior to LLC tumor cell inoculation (*left*, n=16 and 18, respectively; *right*, n=10 and 6, respectively). (D) Representative photomicrographs of anti-CD31 staining of of LLC tumors grown in $S1P_2^{+/+}$ mice which had received BM from either $S1P_2^{+/+}$ or $S1P_2^{-/-}$ donor. Scale bar=100 μm. Microvessel numbers are quantified in high power field (HPF) (*left*).

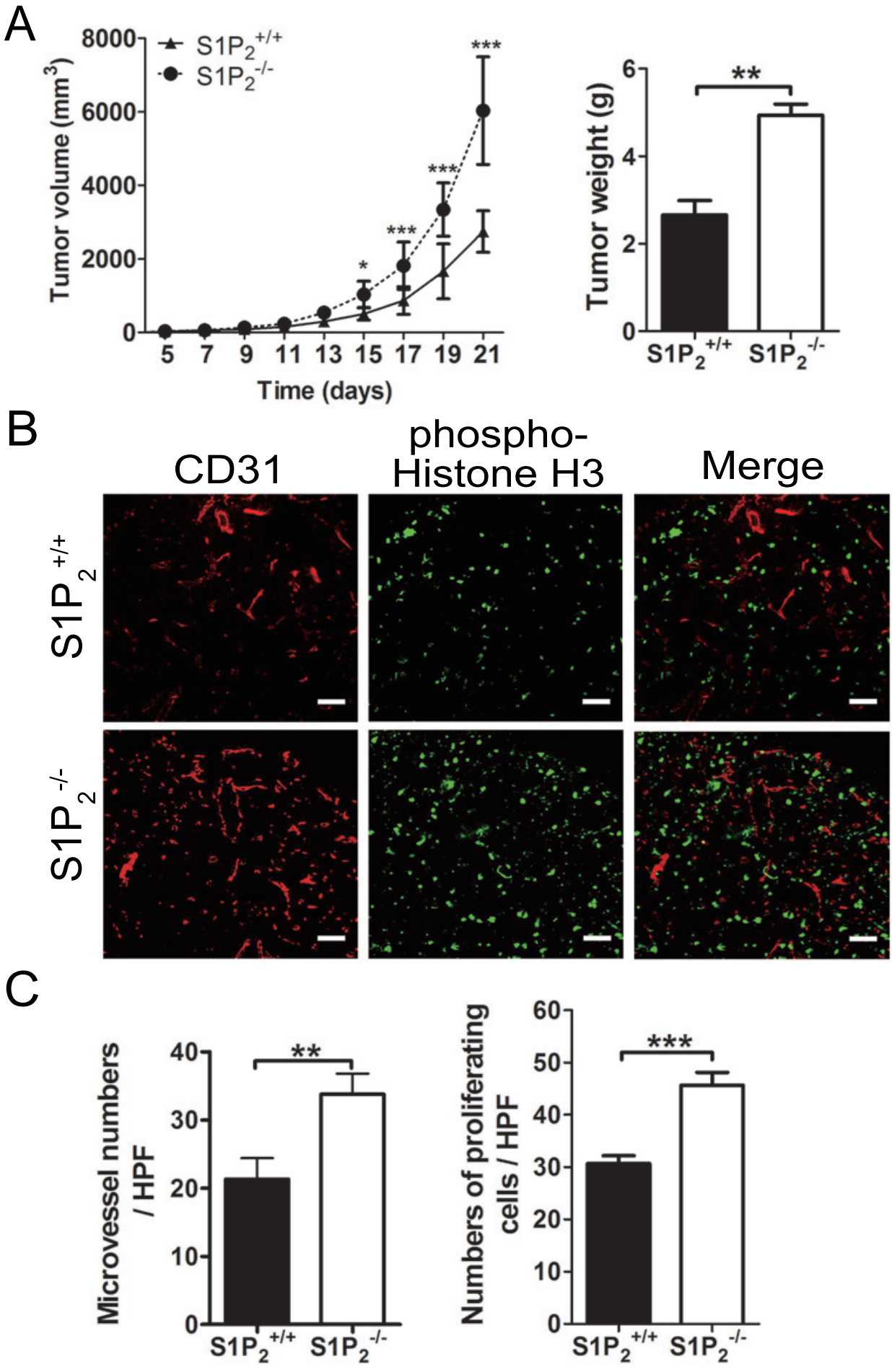

Du et al., Figure 1

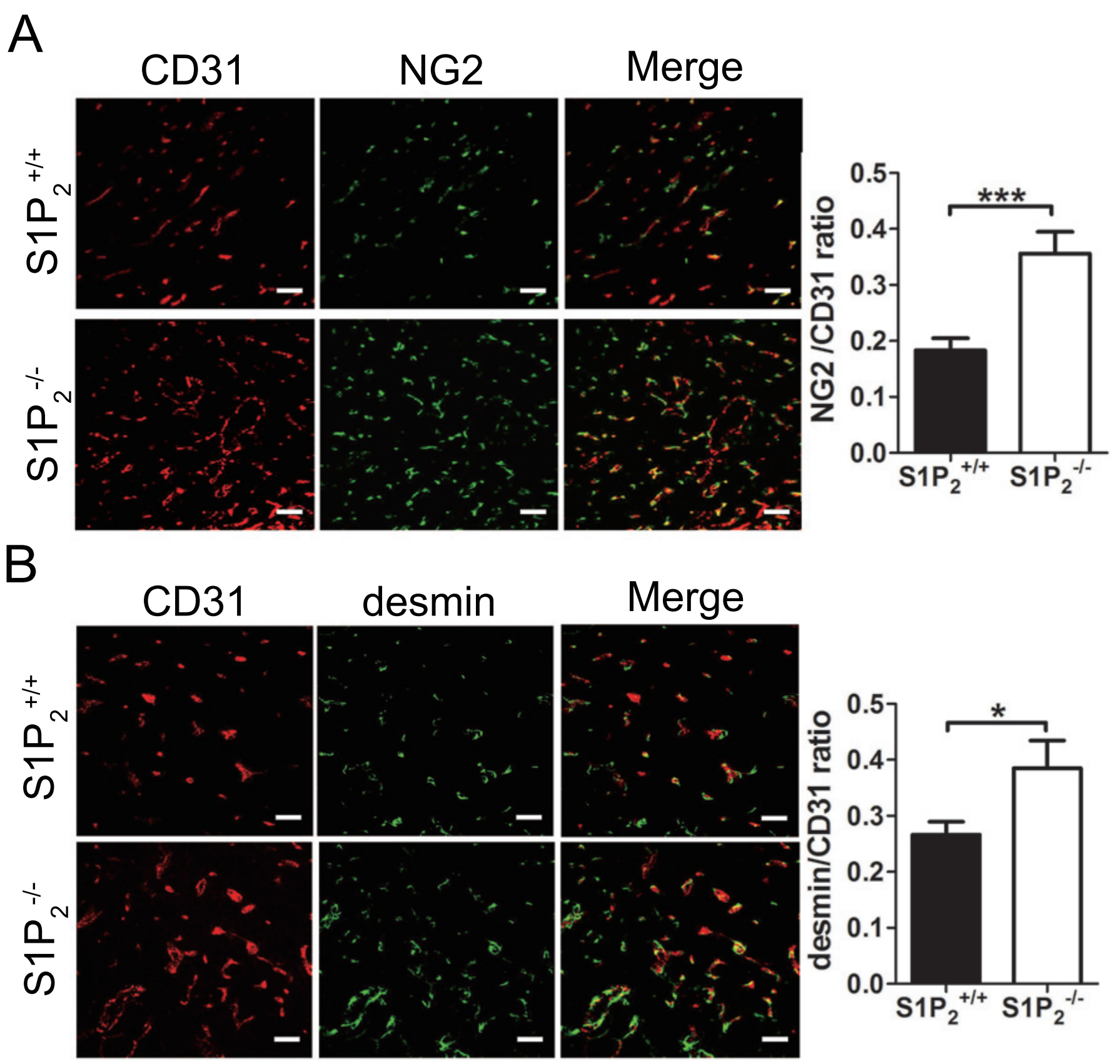

Du et al., Figure 2

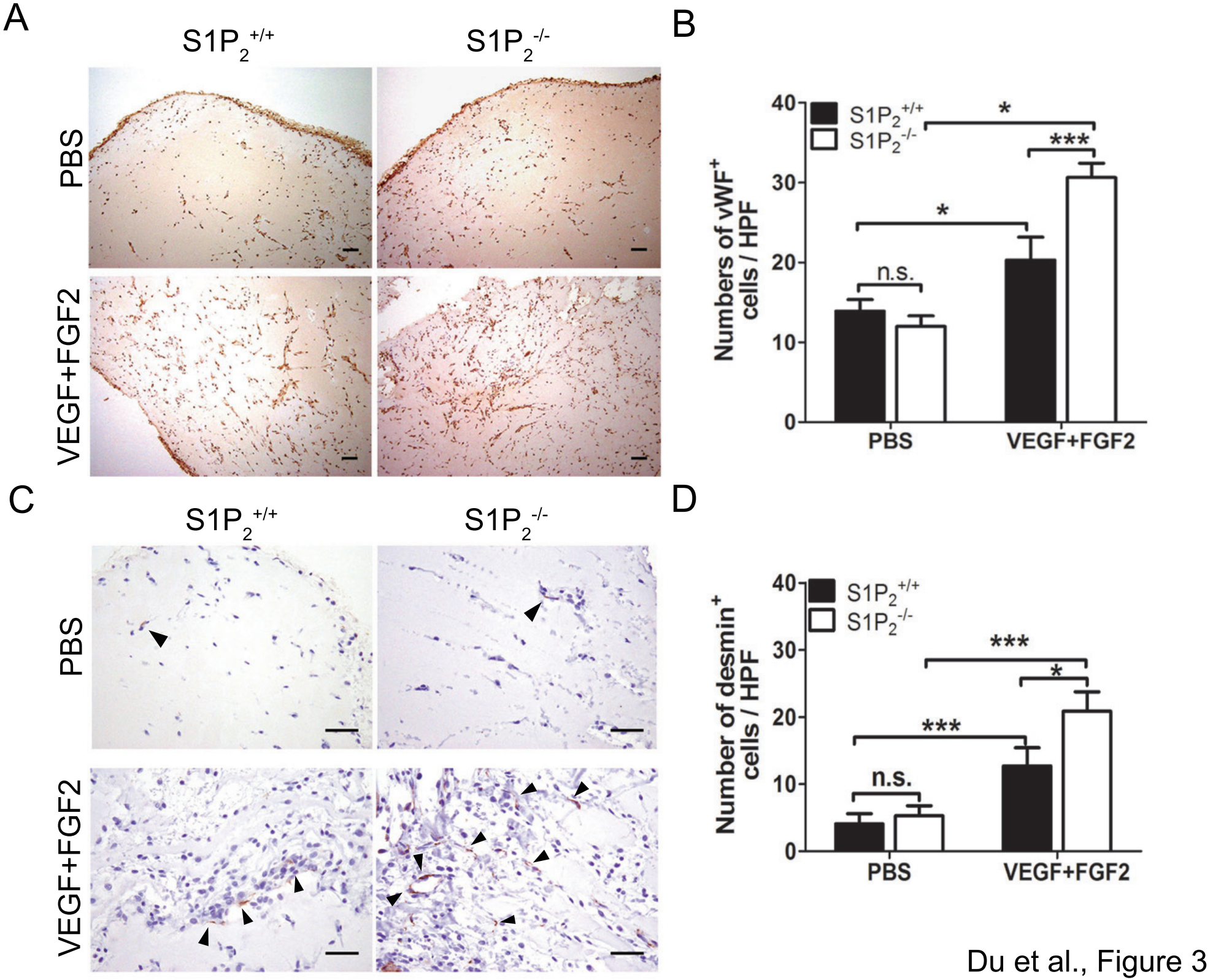

Du et al., Figure 3

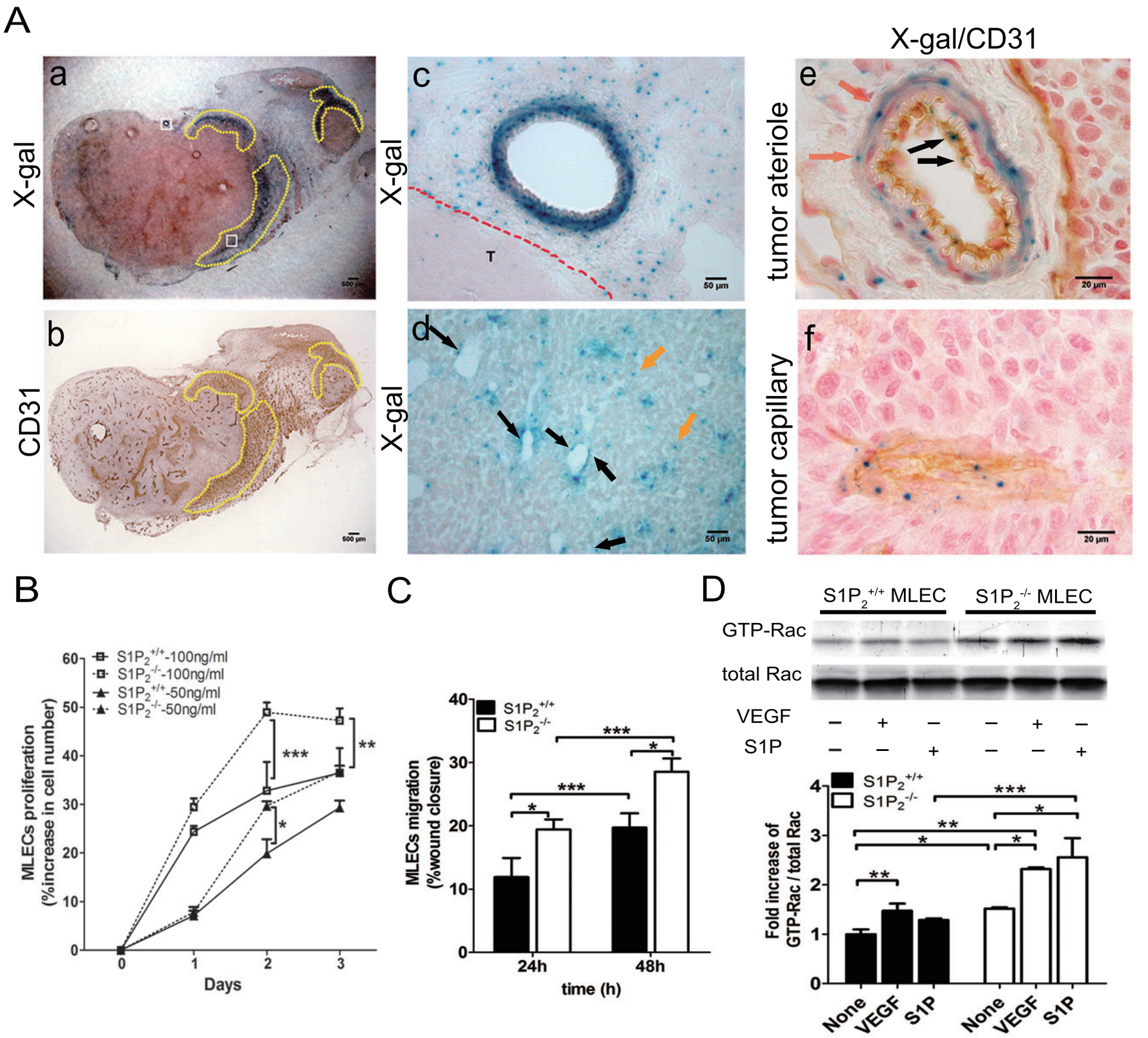

Du et al., Figure 4

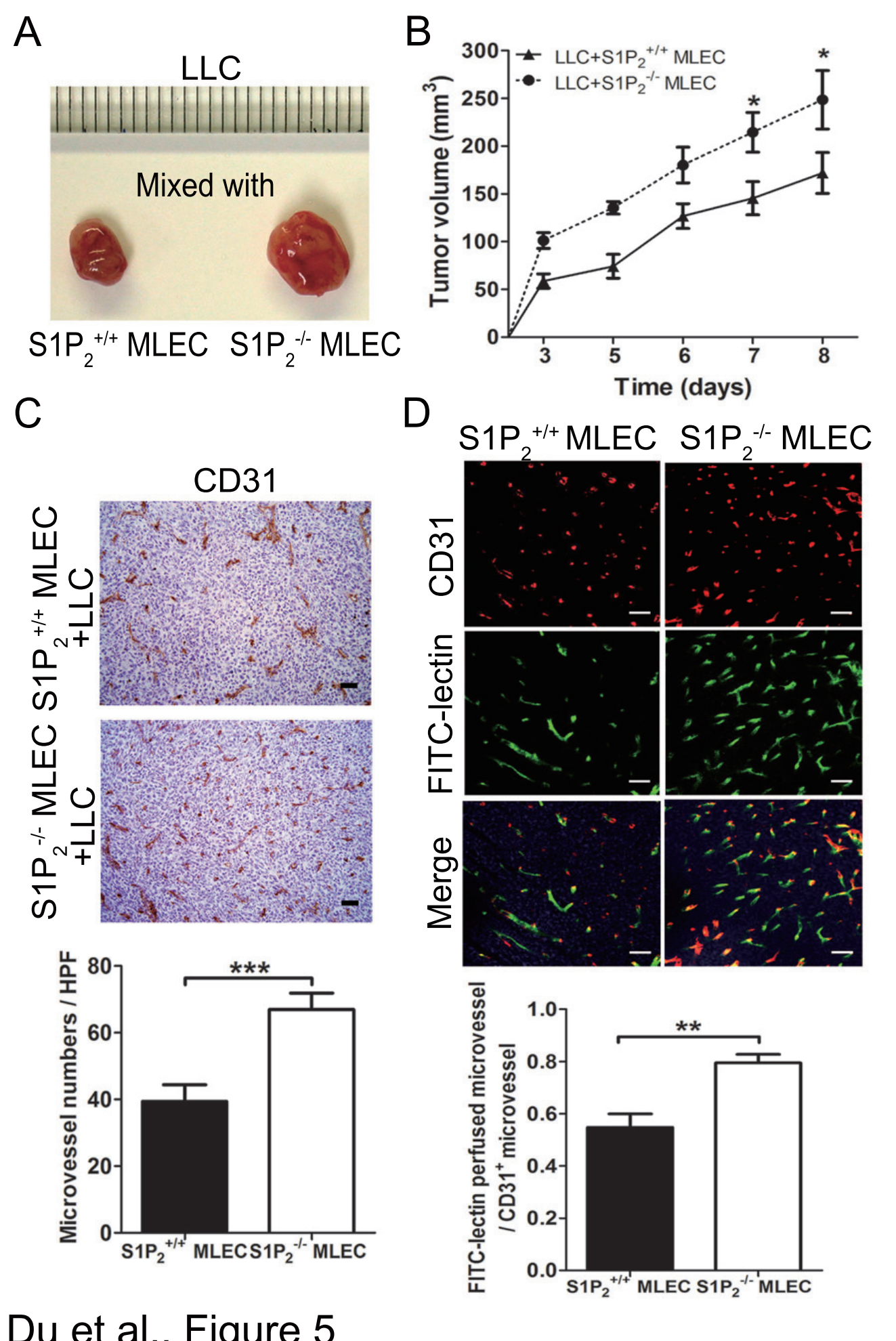

Du et al., Figure 5

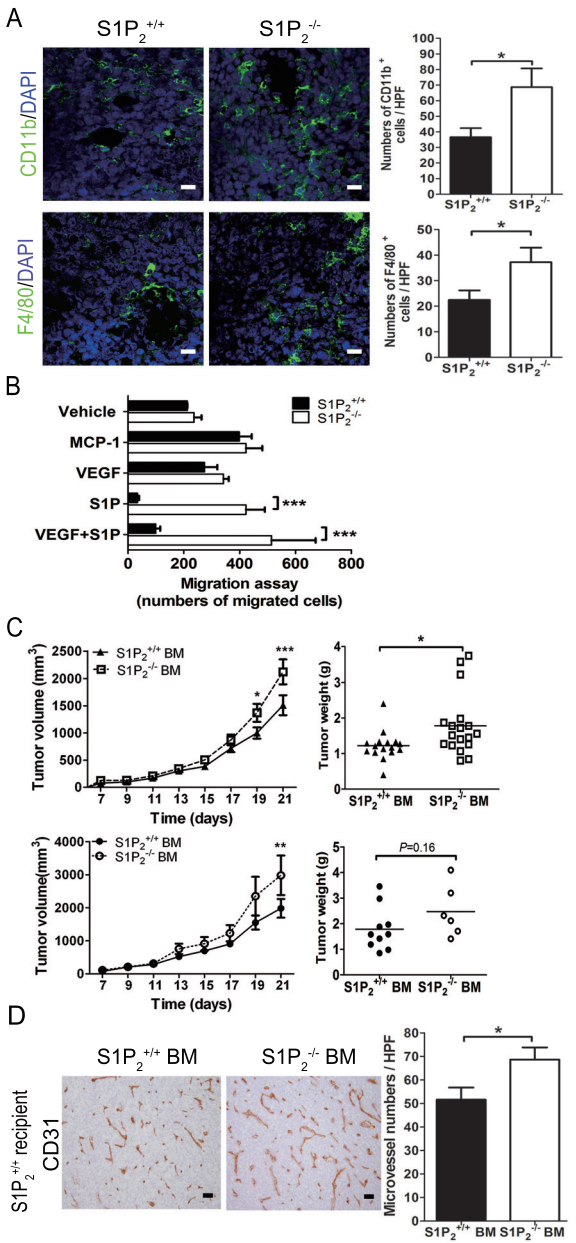

Du et al., Figure 6

Supplemental materials

Generation of $S1P_2$ knockout mice and LacZ knockin mice

For the construction of $S1P_2$ targeting vector, the *S1p2* genomic clones were used along with the plasmid containing a neomycin-resistance cassette (Neo^r) (pMC1Neo vector) and diphtheria toxin-expression cassette (DTA) (pMC1DT-ApA) (1). The DTA gene in the targeting vector was located outside of the homologous sequence to prevent random integration (Supplementary Fig. 1). A 2.8-kb *BglII/BglII* genomic fragment that contains the entire 1.1-kb open reading frame (ORF) of *S1p2*, which was flanked with 5' and 3' flanking regions of 1.1- and 0.6-kb, respectively, was cloned into pLITMUS29 vector. *NaeI* digest of this vector, which lack 0.75-kb 5' region of ORF including the start codon, was ligated with 1.1-kb *BamHI/HincII* fragment of pMC1Neo vector, which resulted in substitution of 0.75-kb 5' region of ORF with Neo gene flanked with thymidine kinase promoter at 5' end. The further ligation of *S1p2* genomic DNA fragments resulted in the targeting vector that contains the 5' (left) and 3' (right) arms of 8.2- and 0.9-kbp sequences, respectively, for homologous recombination. For the construction of $S1P_2$ knockout/lacZ knock-in targeting vector, the previously constructed pLITMUS29 vector containing *S1p2* genomic clone with the partial substitution with the Neo cassette was digested by *BamHI* and ligated with 3.2-kb *NcoI/BamHI* fragment of lacZ/RSV-polyA cassette vector (2). The 5' S1p2 genomic fragment was ligated in frame with the start codon of LacZ DNA in pMCDT-ApA vector with the ligation of the 3' *S1p2* genomic fragment, resulting in the generation of the targeting vector with the identical 5' (left) and 3' (right) arms of *S1p2* genomic sequences to the above-mentioned targeting vector for $S1P_2$ knockout (Supplementary Fig. 2). Details of vector construction are available upon request.

The E14-1 ES cells were electroporated (1.25×107 cells) with 20 μg of linearized DNA and subjected to positive selection with G418 (0.25 mg/ml). For Southern blotting of *NcoI*-digested DNA, the 0.43-kb *BglII-NcoI* DNA fragment located outside of the 3' right arm of the targeting vector (3' probe), which detects 1.6-kb fragment in the targeted *S1p2* allele and 2.1-kb fragment in the wild-type allele, was used. For

$S1P_2$ knockout/LacZ knockin ES cells, the 5' probe (a 0.66-kb *NdeI-NotI* DNA fragment) hybridized to *NdeI*-digested DNA fragments of 11.9- and 9.7-kb fragments in the targeted and wild-type alleles, respectively, and followed by verification with the 3' probe (a 0.85-kb *BglII-BglII* DNA fragment) hybridized to *BamHI*-digested DNA, which detects 2.6- and 6.8-kb fragments in the targeted and wild-type alleles, respectively. The ES cells carrying the targeted alleles were aggregated with 8-cell stage embryos, resulting in male chimeric mice (3). Chimeras were mated with C57BL/6 females to obtain F1 mice carrying each of the targeted alleles. We analyzed S1P2-knockout mice and their littermates on C57BL/6 background (N4) and LacZ knockin mice that were back-crossed to C57BL/6 more than 10 times. We observed seizure attacks in $S1P_2$-knockout mice around the weaning, which resulted in death in 8-10% of mice. This was similar to the previous report (4) but was different from another report which showed that an independently established $S1P_2$-knockout mice did not exhibit seizures or epileptic death during the similar ages (5). We did not observe seizures or epileptic death in backcrossed homozygous LacZ knockin mice. All mice used in this study were bred and maintained at Institute for Experimental Animals, Advanced Science Research Center, Kanazawa University, under specific pathogen-free conditions. All procedures were conducted in accordance with Fundamental Guidelines for Proper Conduct of Animal Experiment and Related Activities in Academic Research Institutions under the jurisdiction of the Ministry of Education, Culture, Sports, Science and Technology of Japan approved by the Committee on Animal Experimentation of Kanazawa University. The guidelines strictly conform to the Guide for the Care and Use of Laboratory Animals published by the US National Institutes of Health (NIH Publication No. 85-23, revised 1996).

Genotyping of $S1P_2$-deficient and LacZ-knockin mice

Mice were genotyped by PCR analysis of genomic DNA prepared from tail biopsies using the primers shown in Supplementary Fig. 1 and 2. The primer sequences were as follows: F1, 5'-cagtgacaaaagctgccgaatgctgatgct-3'; F2, 5'-tggctacccgtgatattgctgaagagcttg-3'; R1, 5'-tgagcagtgagttaagggtggcaaaggcaa-3'. The

PCR conditions were: 33 cycles of 94°C (30 sec), 59°C (45 sec), 72°C (30 sec) for F1 and R1, and 33 cycles of 94°C (30 sec), 59°C (45 sec), 72°C (30 sec) for F2 and R1. The amplified products were 424-bp in the wild-type allele and 241-bp in the targeted alleles in $S1P_2$-knockout mice and LacZ-knockin mice.

Tumor blood vessel perfusion analysis

Vascular perfusion was visualized by injecting fluorescent isothiocyanate (FITC)-conjugated dextran (Sigma) via tail vein at a dose of 2 mg/kg and harvesting tumors after 1h.

Tube formation assay

Capillary-like tube formation was performed as described previously (6), and the obtained images were analyzed for the average number of tube branching points and tube length by using Image J software (NIH).

Reverse transcription (RT)-PCR and Real-time PCR

Total RNA was isolated from LLC tumors grown in either $S1P_2^{+/+}$ or $S1P_2^{-/-}$ mice for 7-days using TRIZOL reagent (Invitrogen, USA). One microgram of total RNA was transcribed into first-strand cDNA using oligo(dT) 18 primer and ReverTraAce (Toyobo, Japan) according to the manufacturer's instructions. One μl of the reaction mix (out of 25 μl in total) was amplified by PCR conducted for 25-28 cycles with reverse transcribed DNA as template. The extract without RT reaction was used as a template for the negative control. After amplification, PCR products were separated on 2% agarose gels and visualized by ethidium bromide staining. They were determined from the 3 independent experiments and normalized for expression levels of GAPDH mRNA (20 cycles of PCR). Sequences of specific primers and amplified product sizes are listed in Supplementary Table 1.

Quantitative real-time PCR was performed using the 7300 real-time PCR System and the Assays-on-Demand Gene Expression product (Taqman, Mammalian Gene Collection probes) according to the manufacture's instructions (Applied Biosystems).

Primers for murine VEGF (Vegfa, Mm00437308_m1), TGFβ (Tgfb1, Mm00441726_m1), bFGF (Fgf2, Mm00433287_m1), IL-1β (Il1b, Mm00434228_m1), angiopoitin-1 (Angpt1, Mm00456498_m1), PDGF-B (Pdgfb, Mm01298578_m1), HGF (Hgf, Mm01135185_m1), CXCL12 (Cxcl12, Mm00445553_m1), S1P1 (S1p1r, Mm00514644_m1), S1P3 (S1p3r, Mm00515669_m1), VEGFR1(flt1, Mm00438980), VEGFR2(kdr, Mm00440099_m1) were also obtained from Applied Biosystems. TaqMan Rodent Glyceraldehyde-3-phosphate Dehydrogenase (GAPDH) Control Reagents (Applied Biosystems) were used as an endogenous control. ΔCt was calculated as (gene of interest Ct) − (*GAPDH* Ct) using Sequence detector (Applied Biosystems) and Microsoft Excel (Microsoft corp., Redmond, WA, USA). The relative quantity of mRNA of gene of interest was calculated by $\Delta\Delta$Ct calculation as $2^{-((\Delta\text{Ct of S1P2-/- sample})-(\Delta\text{Ct of S1P2+/+ sample}))}$. The amplification efficiencies of the target and the endogenous reference were confirmed by observing the equal relationship between cDNA dilution and ΔCt. All experiments included negative controls consisting of no cDNA for each primer pair.

S1P1/CD31 double immunofluorescent staining

S1P1 polyclonal antibody was provided by Dr. S. Mandala (Merck).

Western blotting

MLECs were serum-starved in M199 medium with 0.5% BSA (fatty acid free) for 36 h before stimulation with VEGF (100 ng/ml) or S1P (10^{-7} M) for 10 minutes. Cells were rinsed with ice-cold PBS and lysed in 2× Laemmli's loading buffer and subjected to Western blotting with antibodies against phospho-Akt (#4060, Cell signaling), total Akt (#9272, Cell signaling), phospho-ERK1/2 (#4370, Cell signaling), and total ERK1/2(#9102, Cell signaling).

References:

1. Yagi T, Nada S, Watanabe N, et al. A novel negative selection for homologous recombinants using diphtheria toxin A fragment gene. Anal Biochem. 1993; 214(1): 70-6.
2. Sugaya T, Nishimatsu S, Tanimoto K, et al. Angiotensin II Type 1a Receptor-deficient Mice with Hypotension and Hyperreninemia. J Biol Chem. 1995; 270(32): 18719-18722.
3. Asano M, Furukawa K, Kido M, et al. Growth retardation and early death of beta-1,4-galactosyltransferase knockout mice with augmented proliferation and abnormal differentiation of epithelial cells. EMBO J. 1997; 16(8): 1850-1857.
4. MacLennan AJ, Carney PR, Zhu WJ, et al. An essential role for the H218/AGR16/Edg-5/LP(B2) sphingosine 1-phosphate receptor in neuronal excitability. Eur J Neurosci. 2001; 14(2): 203-9.
5. Ishii I, Ye X, Friedman B, et al. Marked perinatal lethality and cellular signaling deficits in mice null for the two sphingosine 1-phosphate (S1P) receptors, S1P(2)/LP(B2)/EDG-5 and S1P(3)/LP(B3)/EDG-3. J Biol Chem. 2002; 277(28): 25152-9.
6. Inoki I, Takuwa N, Sugimoto N, et al. Negative regulation of endothelial morphogenesis and angiogenesis by S1P2 receptor. Biochem Biophys Res Commun 2006; 346: 293-300.

Supplementary Figure Legends

Supplementary Figure 1. Generation of $S1P_2$ knockout mice. (A) $S1P_2$ knockout mice were generated as described in "Generation of $S1P_2$ knockout mice and $S1P_2$ knockout/lacZ knock-in mice." (B) Southern blot analysis of $S1P_2$ knockout mouse genomic DNA. The wild type and the targeted alleles show 2.1- and 1.6-kb fragments hybridized by the probe. (C) Northern blot analysis shows that the expression levels of $S1P_1$ and $S1P_3$ mRNAs were similar in $S1P_2^{+/+}$ and $S1P_2^{-/-}$ mice.

Supplementary Figure 2. Generation of $S1P_2$ knockout/lacZ knock-in mice. (A) $S1P_2$ lacZ knockin mice were generated as described in "Generation of $S1P_2$ knockout mice and $S1P_2$ knockout/lacZ knock-in mice." (B) Southern blot analysis of $S1P_2$ knockout/lacZ knock-in mouse genomic DNA. The wild type allele shows 9.7 kb (5' probe) and 6.8-kb (3' probe) bands, and the targeted allele shows 11.9-kb (5' probe) and 2.6-kb (3' probe) bands, respectively. (C) Genotyping of wild type, heterozygous and knockout mice by PCR using tail genomic DNA. The amplified PCR products were 424-bp and 241-bp in the wild-type and the targeted alleles, respectively.

Supplementary Figure 3. Increased tumor angiogenesis and tumor cell proliferation in B16BL6 melanoma grown in $S1P_2$ deficient mice. (A) Tumor volumes of B16BL6 inoculated subcutaneously in $S1P_2^{+/+}$ (solid lines) and $S1P_2^{-/-}$ (dotted lines) littermate mice were measured every other day (n=14). (B) Tumor blood vessels and proliferating cell nuclei were detected by anti-CD31 (red) and anti-phospho-Histone H3 (green) double immunofluorescence. Representative images are shown. (C) The numbers of tumor microvessels (*left*) and proliferating cell nuclei (*middle*) were counted in each high power field (HPF) (n=6). (D) Intravenously administered FITC-dextran (green) was detected in LLC tumors grown in $S1P_2^{+/+}$ and $S1P_2^{-/-}$ mice under a fluorescent microscope. White arrows, tumor microvessels identified with functional perfusion. Scale bar=100 μm. The pixels of FITC-dextran per high power field (HPF) were quantified (*right*).

Supplementary Figure 4. Upregulation of vascular gene expression in LLC tumors grown in $S1P_2$ deficient mice. The mRNA expression levels of CD31, VE-cadherin, VEGFR2, Notch1 were determined by RT-PCR. Data are representative of three independent experiments. GAPDH served as the internal control. The data (means ± SEM) are shown as -fold changes over the values in tumors of $S1P_2^{+/+}$ mice, which are expressed as 1.0. Sequences of specific primers are listed in Supplementary Table 1.

Supplementary Figure 5. $S1P_2$ is mainly expressed in blood vessels of various tissues in adult $S1P_2^{LacZ/+}$ mice. (A) X-gal staining of $S1P_2^{LacZ/+}$ mouse tissues including lung, brain, skeletal muscle, kidney, liver, and bone marrow. Scale bars=100 μm. (B) Double staining for LacZ activity and CD31 immunoreactivity disclosed that $S1P_2$ is expressed widely in all adult $S1P_2^{LacZ/+}$ mouse tissues examined. The major cells that are positive for LacZ activity are vascular endothelial cells and smooth muscle cells in many tissues. The arrowheads in skeletal muscle indicate capillaries and larger sizes of vasculatures. In the liver, V, central vein; P, portal vein; A, artery.

Supplementary Figure 6. Mouse lung endothelial cells (MLECs) isolated from $S1P_2^{-/-}$ mice showed increased cell migration and tube formation *in vitro*. (A) Primary cultures of MLECs isolated from $S1P_2^{LacZ/+}$, $S1P_2^{+/+}$ and $S1P_2^{-/-}$ mouse lungs, in which either LacZ activity (*left*) or VE-cadherin (*middle* and *right*) was detected by X-gal staining and immunofluorescence staining, respectively. Scale bars: 100 μm (X-gal staining) and 20 μm (anti-VE-cadherin immunofluorescence), respectively. (B) Representative photomicrographs of *in vitro* wound healing assay. (C) *Left*, representative photomicrographs of *in vitro* tube formation assay in the presence of 2% fetal bovine serum (FBS) alone (control) and 2% FBS plus 100 ng/ml VEGF (VEGF). *Right*, the tube formation by MLECs isolated from $S1P_2^{LacZ/+}$ mice in the presence of 2% FBS plus VEGF is visualized by X-gal staining. (D) Numbers of branching points and total tubular length in the presence or absence of VEGF were

quantified from tube formation assay.

Supplementary Figure 7. $S1P_1$ expression in LLC tumor isograft and the expression of $S1P_1$ and $S1P_3$ in $S1P_2^{+/+}$ and $S1P_2^{-/-}$ MLECs. (A) Immunofluorescence staining of $S1P_1$ and CD31 in LLC tumor isografts. There is no difference in $S1P_1$ expression in tumor blood vessels between $S1P_2^{+/+}$ and $S1P_2^{-/-}$ mice. (B)Total RNA was isolated from $S1P_2^{+/+}$ and $S1P_2^{-/-}$ MLECs. The mRNA expression levels of $S1P_1$, $S1P_3$, and VEGFR2 were determined by real-time PCR. Data are representative of three independent experiments. The data (means ± SEM) are shown as -fold changes over the values in $S1P_2^{+/+}$ MLECs, which are expressed as 1.0.

Supplementary Figure 8. Phosphorylation of Akt and ERK in $S1P_2^{+/+}$ and $S1P_2^{-/-}$ MLECs. (A) and (B), MLECs from the $S1P_2^{+/+}$ and $S1P_2^{-/-}$ were starved 36h in M199 medium plus 0.5% BSA (fatty acid free), and then stimulated with VEGF (100ng/ml) or S1P (10^{-7} M) for 10 minutes. Cell lysates were subjected to Western blotting using antibodies against phospho-Akt, total Akt (A), phospho-ERK1/2, and total ERK1/2 (B) as described in Supplementary Materials. *Right*, representative blots are shown. *Lef*t, the quantitative analyses. The data (means ± SEM) are shown as -fold increases above the basal levels in $S1P_2^{+/+}$ MLECs, which are expressed as 1.0.

Supplementary Figure 9. $S1P_2$ deficient MLECs co-injected with B16BL6 tumor cells promote tumor growth *in vivo*. (A) Representative images (*left*) and growth curves (*right*) of B16BL6 tumors, which had been implanted together with either $S1P_2^{+/+}$ or $S1P_2^{-/-}$ MLECs (1×10^6 tumor cells mixed with 2×10^5 MLECs) into wild-type mice. (B) Representative X-gal staining image of LLC with $S1P_2^{LacZ/LacZ}$ MLECs co-injected to wild-type mouse.

Supplementary Figure 10. X-gal staining and immunostaining for myeloid cell markers of LLC tumor sections from $S1P_2^{LacZ/+}$ mice. LLC tumor cells were

inoculated into $S1P_2^{+/+}$ mice that had received transplantation of bone marrow (BM) cells from $S1P_2^{LacZ/+}$ mice at 5 weeks prior to LLC cell inoculation, and tumors were excised at 21 days. (A), Sections of LLC tumors were probed with X-gal staining and counterstained with nuclear fast red. (B)-(D), Sections of LLC tumors were subjected to double staining of X-gal and immunohistochemistry using either anti-CD31 (B), anti-CD11b (C) or anti-Gr-1 (D). (A) Tumor peripheral region shows a scattered pattern of abundant infiltration of X-gal staining-positive BMDCs, scale bar=100 μm. (B) CD31-positive vascular endothelial cells are negative for X-gal staining. X-gal staining-positive cells are localized in the tumor stroma outside the blood vessel (*black arrowheads*). (C) Co-localization of LacZ activity (*black arrowheads*) and $CD11b^+$ (*red arrowheads*). All X-gal-positive cells in the high power field are also positive for CD11b staining. (D) Independent expression of LacZ activity (*black arrowheads*) and Gr-1 (*red arrowheads*). Scale bar=20 μm.

Supplementary Figure 11. Upregulation of angiongenesis-related gene expression in LLC tumors grown in $S1P_2$ deficient mice. The mRNA expression levels of angiogenic factors and related molecules were determined by real-time PCR. The mRNA expression of VEGF-A, TGFβ1, bFGF, IL-1β differed between $S1P_2^{+/+}$ and $S1P_2^{-/-}$ mice. The data (means ± SEM) are shown as -fold changes over the values in tumors of $S1P_2^{+/+}$ mice, which are expressed as 1.0, and representative of three independent experiments.

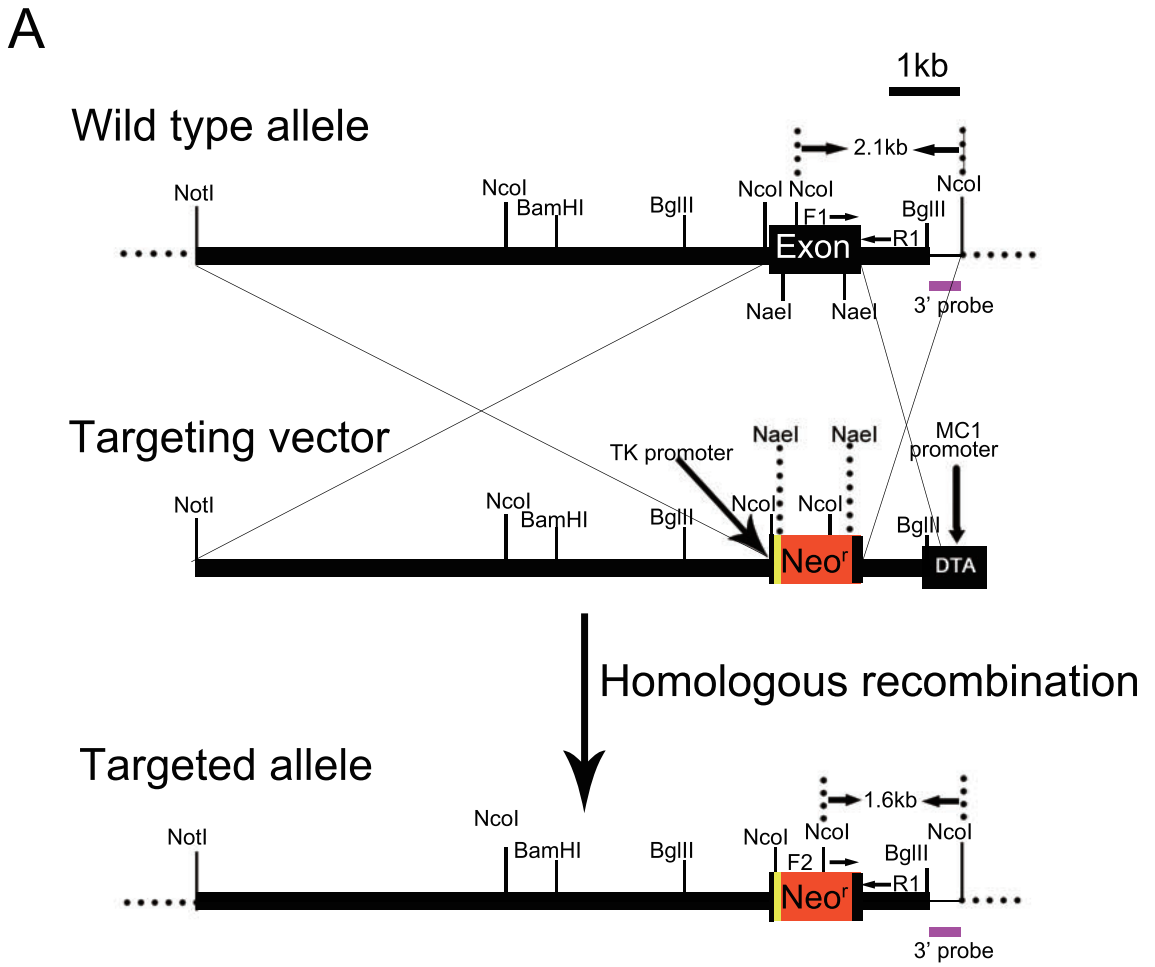

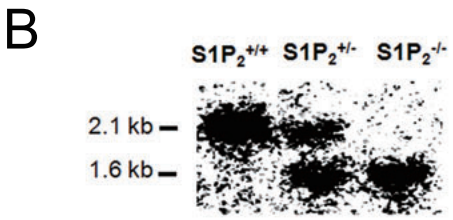

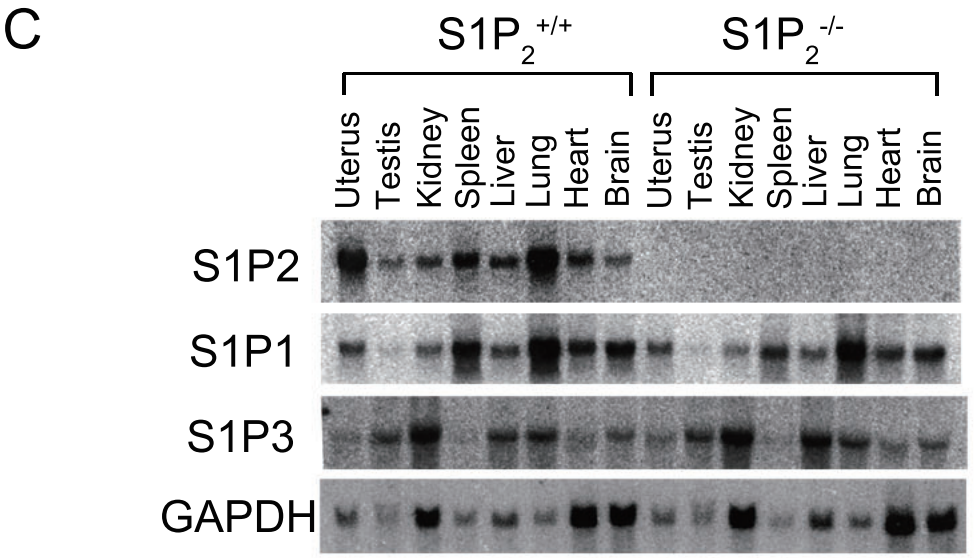

Suppl. Figure 1

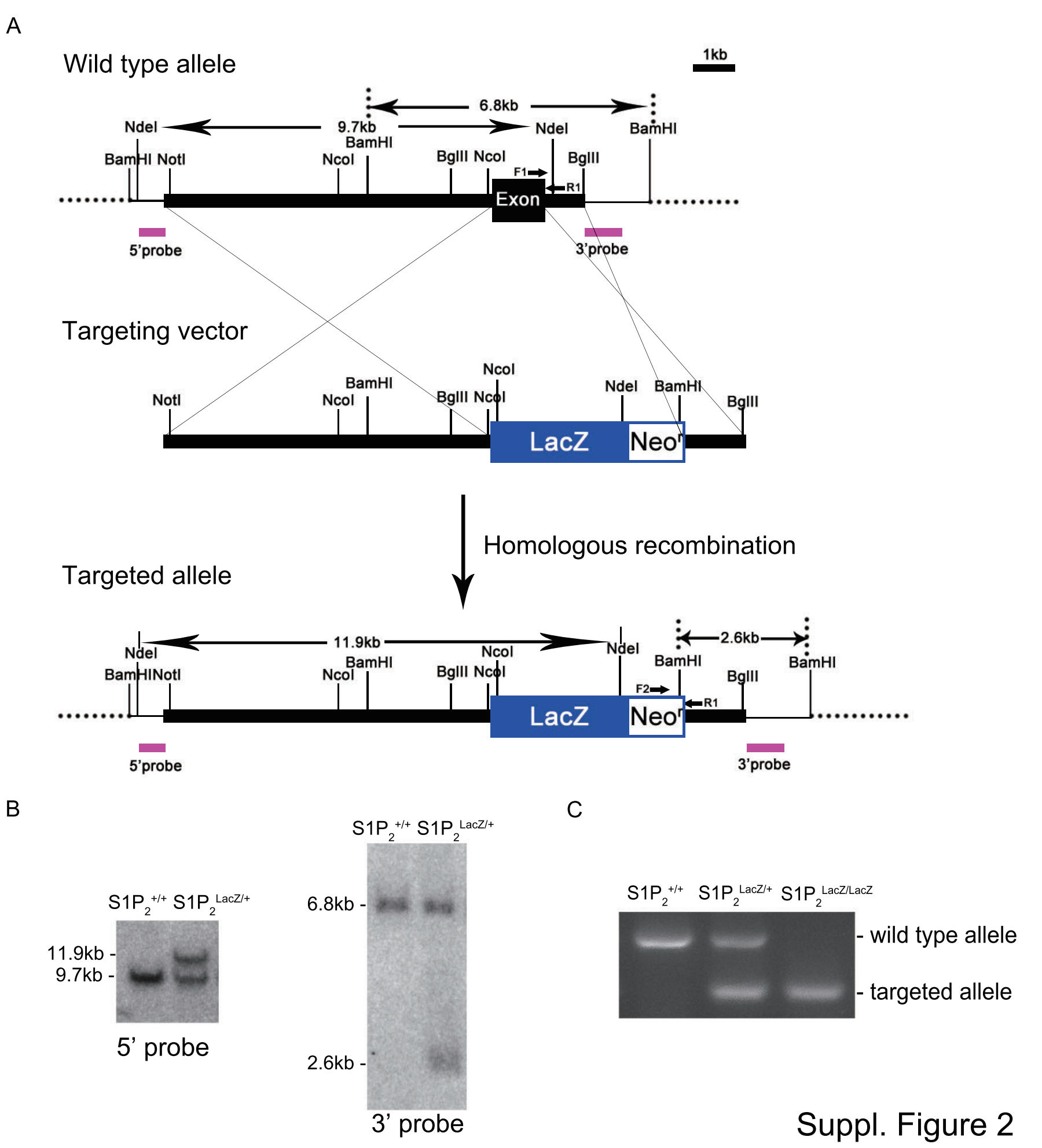

Suppl. Figure 2

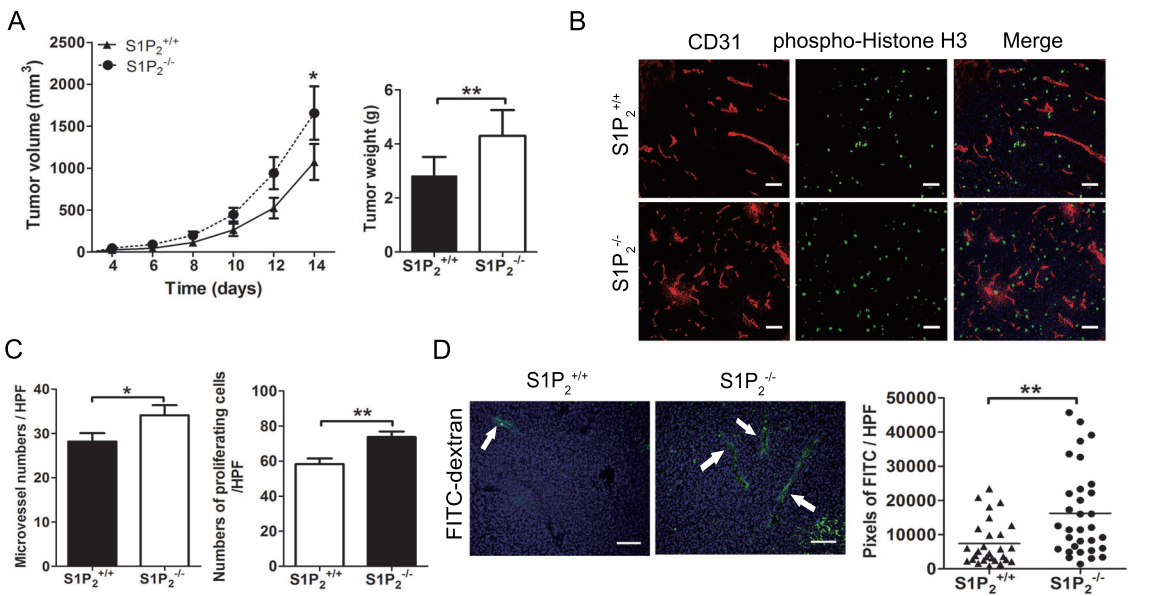

Suppl. Figure 3

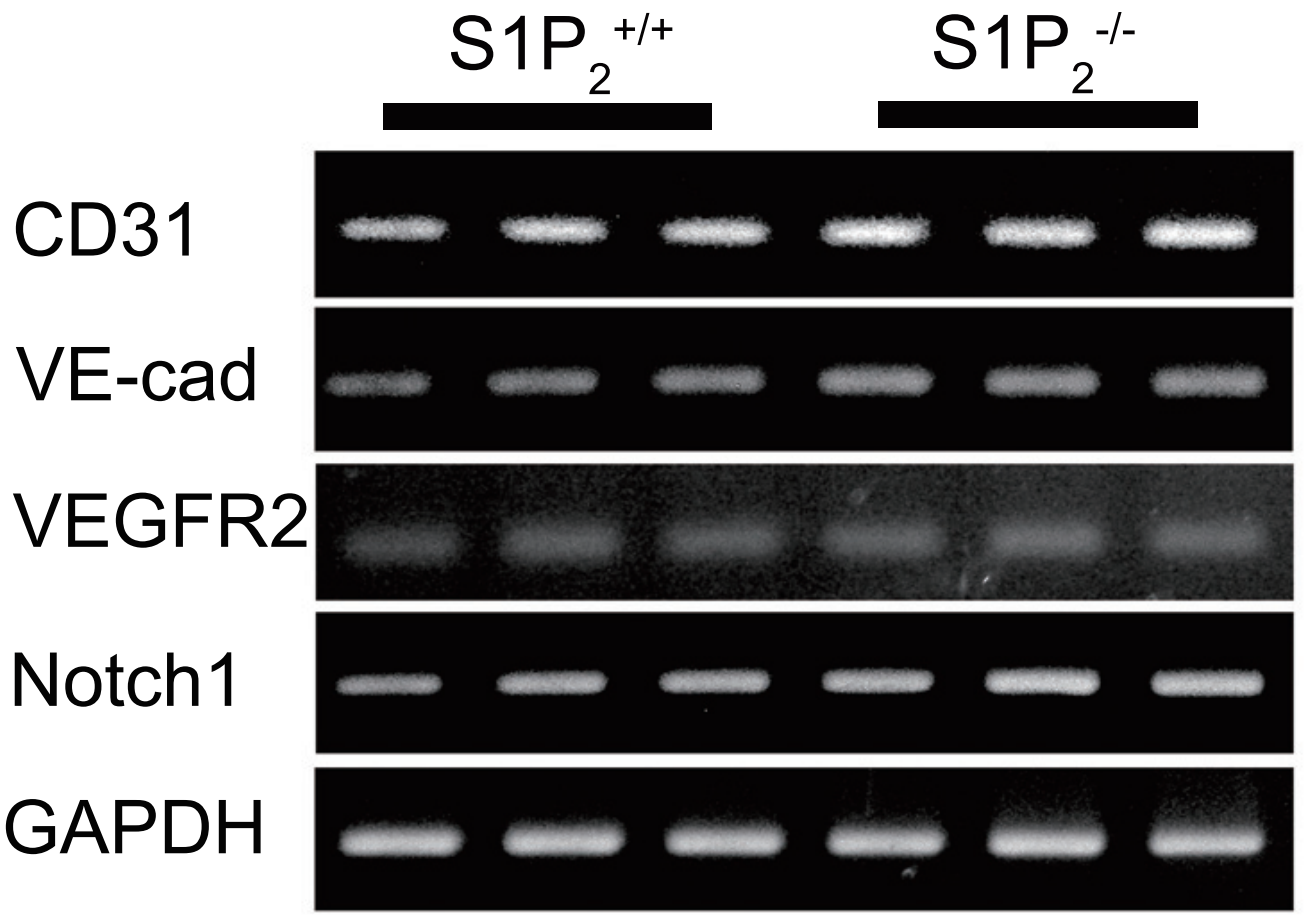

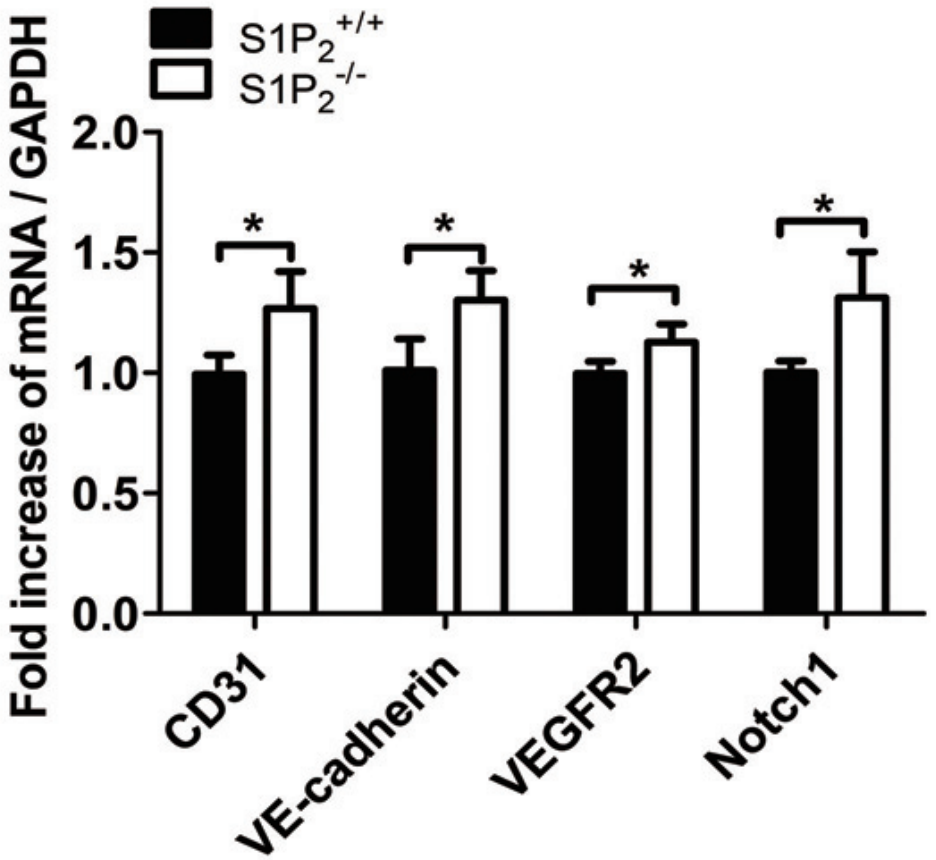

Suppl. Figure 4

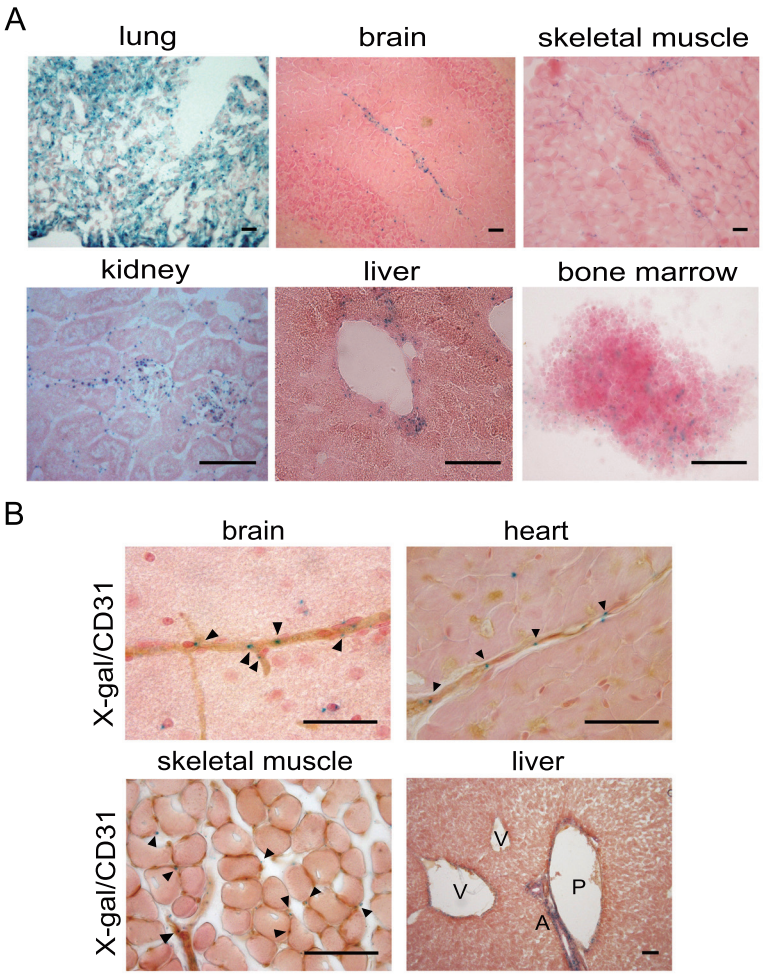

Suppl. Figure 5

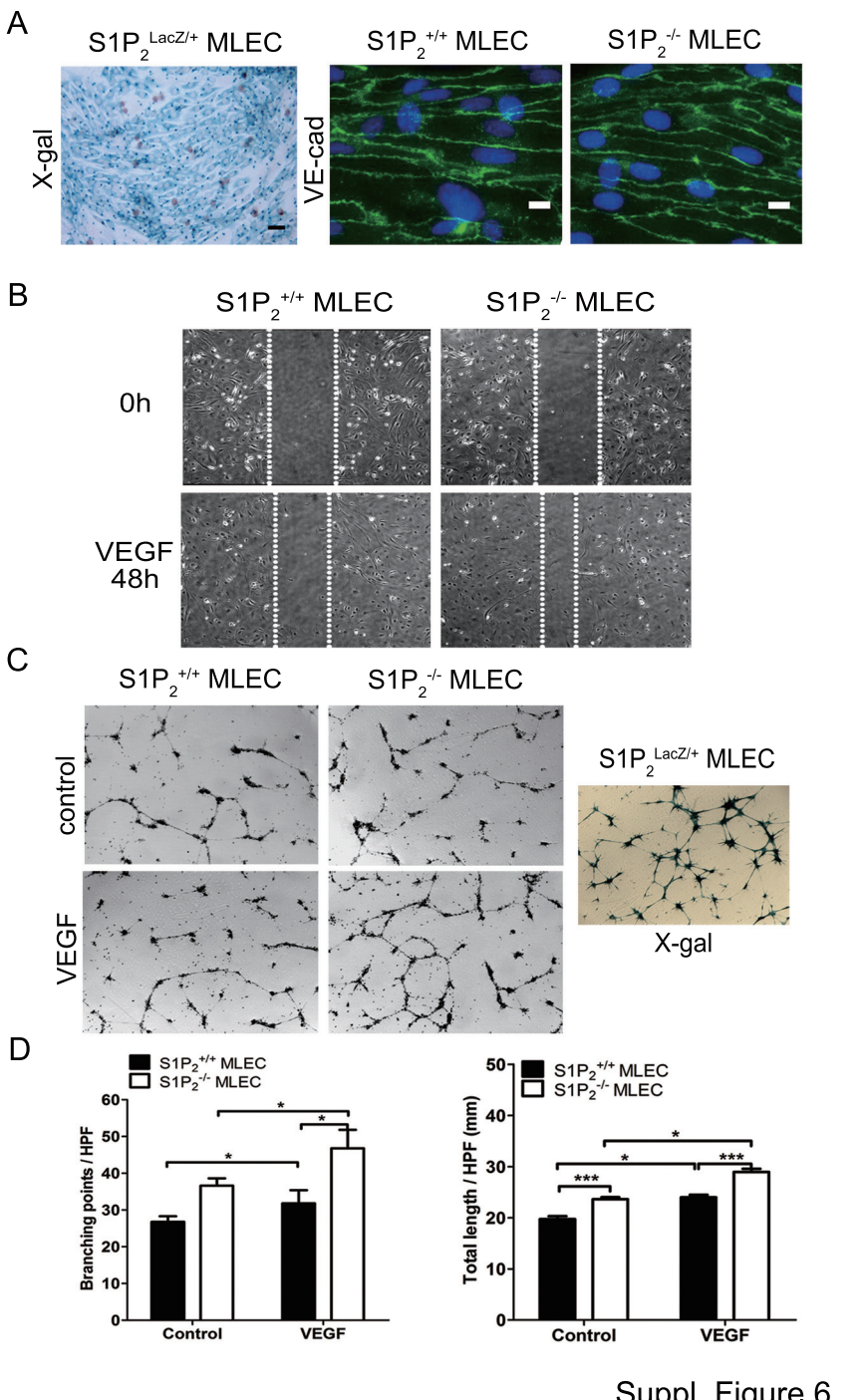

Suppl. Figure 6

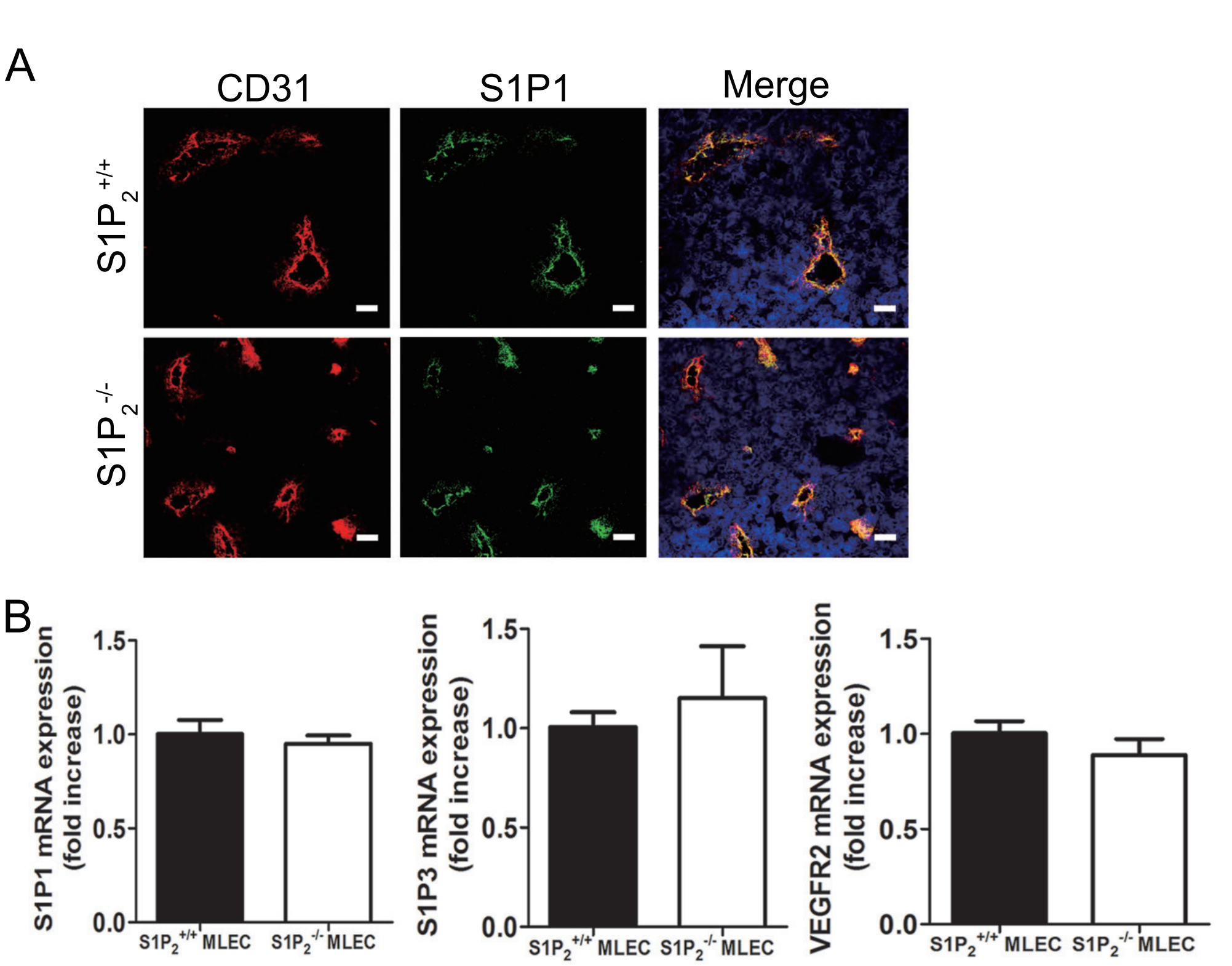

Suppl. Figure 7

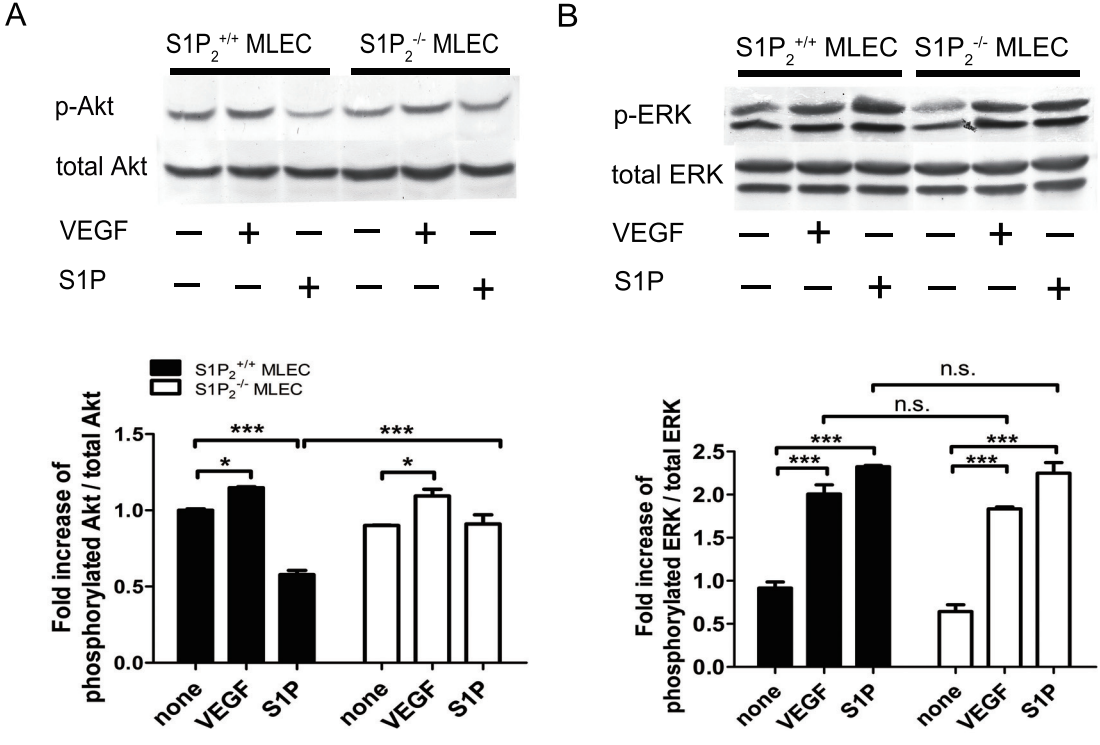

Suppl. Figure 8

A

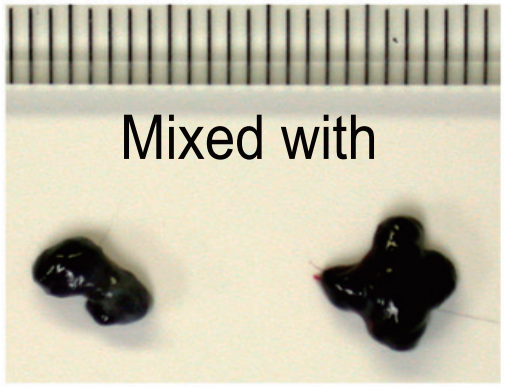

$S1P_2^{+/+}$ MLEC $S1P_2^{-/-}$ MLEC

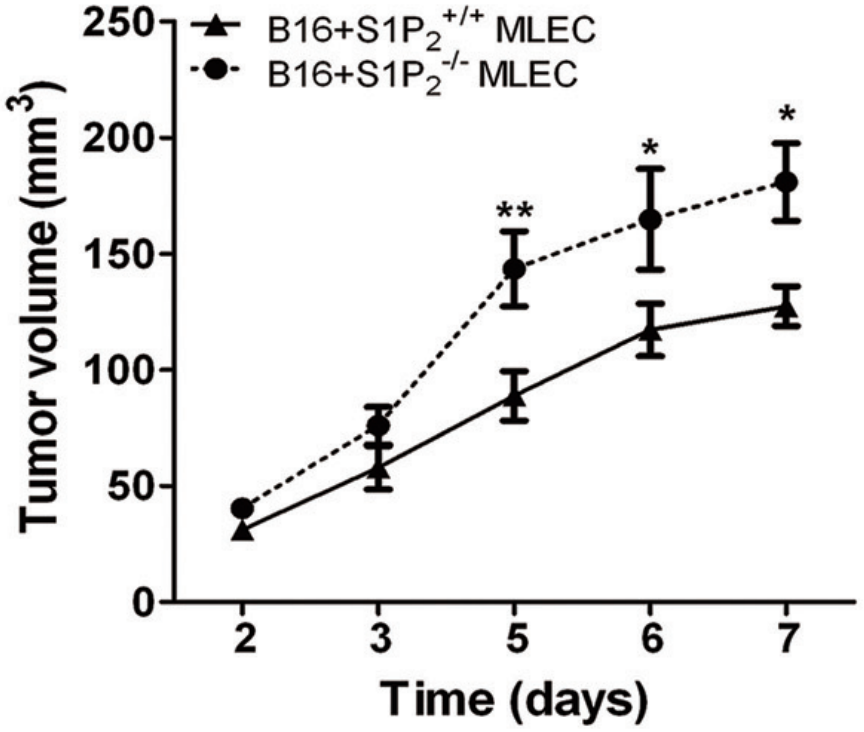

B

$S1P_2^{+/+}$

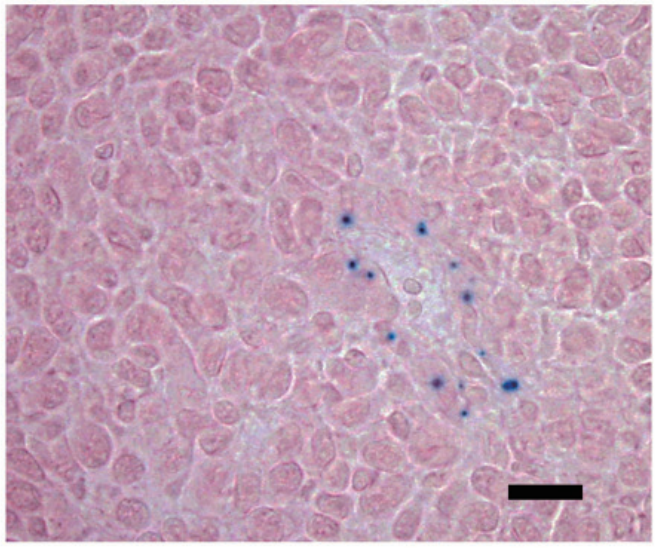

$S1P_2^{lacZ/LacZ}$ MLEC + LLC co-injection

Suppl. Figure 9

$S1P_2^{LacZ/+}$ BM
$S1P_2^{+/+}$ recipient

X-gal

X-gal/CD31

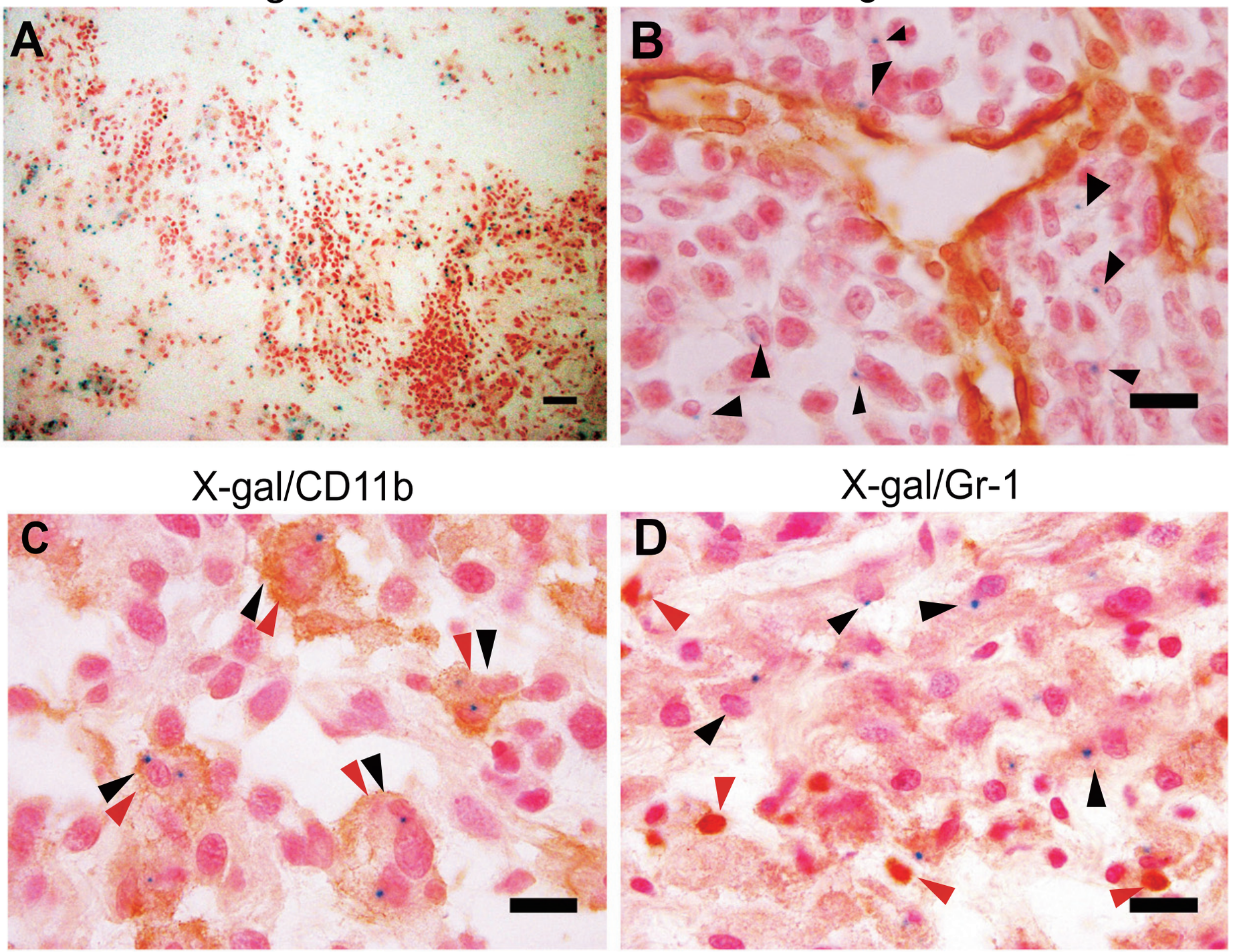

X-gal/CD11b

X-gal/Gr-1

Suppl. Figure 10

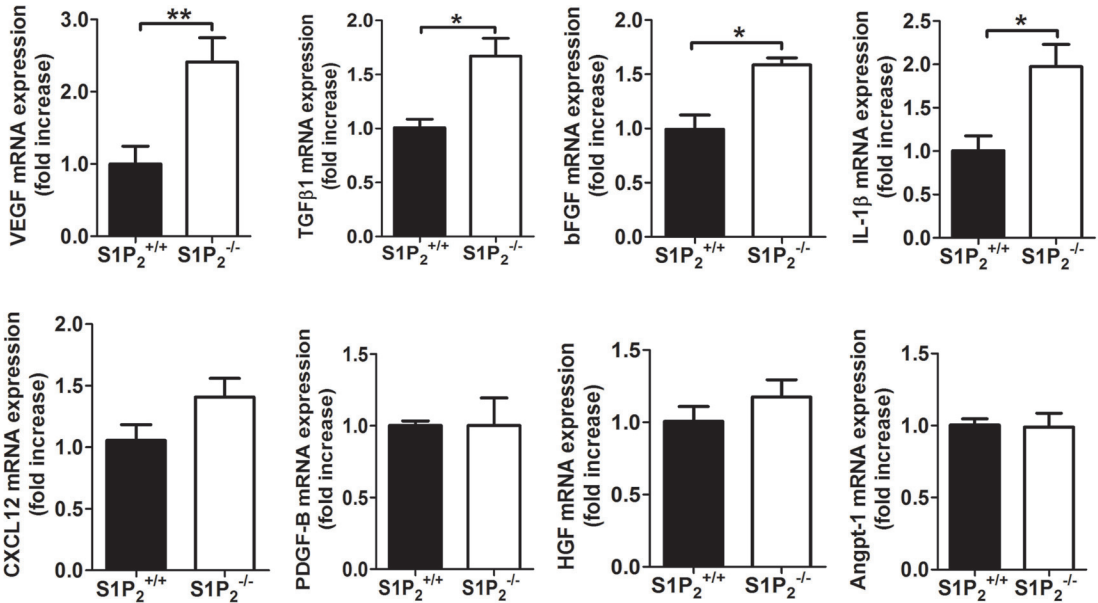

Suppl. Figure 11

Supplementary Table 1

Targets	Primers	Sequences	Targets	Primers	Sequences
CD31*	sense	5'-TCCCTGGGAGGTCGTCCAT-3'	MMP-2	sense	5'-AAGGATGGACTCCTGGCACATGCCTTT-3'
	antisense	5'-GAACAAGGCAGCGGGGTTTA-3'		antisense	5'-ACCTGTGGGCTTGTCACGTGGTGT-3'
VE-cad*	sense	5'-ACGGACAAGATCAGCTCCTC-3'	MMP-9	sense	5'-GTGGTATAGTGGGACACATAGTGG-3'
	antisense	5'-TCTCTTCATCGATGTGCATT-3'		antisense	5'-GTGGTATAGTGGGACACATAGTGG-3'
VEGFR2*	sense	5'-TACACAATTCAGAGCGATGTGTGGT-3'	MT1-MMP	sense	5'-TGCGACGGGAACTTTGACACCG-3'
	antisense	5'-CTGGTTCCTCCAATGGGATATCTTC-3'		antisense	5'-TCCTCCTCAGTCCCCTCATC-3'
Notch1*	sense	5'-GGATCACATGGACCGATTGC-3'	PAI-1*	sense	5'-GACACCCTCAGCATGTTCATC-3'
	antisense	5'-CCACATCTGACAAGTAGCCATG-3'		antisense	5'-AGGGTTGCACTAAACATGTCAG-3'
Dll4*	sense	5'-AGCTGGAAGTGGACTGTGGT-3'	TGFβRII	sense	5'-GGAAGTCTGCGTGGCCGTGTGG-3'
	antisense	5'-TAGAGTCCCTGGGAGAGCAA-3'		antisense	5'-CTATGGCAATCCCCAGCGGAGG-3'
Ang-2	sense	5'-CACACTGACCTTCCCCAACT-3'	VEGFR1	sense	5'-GAGGAGGATGAGGGTGTCTATAGG-3'
	antisense	5'-TGGTGTCTCTCAGTGCCTTG-3'		antisense	5'-TGATCAGCTCCAGGTTTGACTTG-3'
Tie-2	sense	5'-GGACAGTGCTCCAACCAAATG-3'	Neruoplin	sense	5'-ACTGACAGCGCAATAGCAAAAGAAG-3'
	antisense	5'-GACGGAAATGTTGAAAGGC-3'		antisense	5'-TCGGACAAATCGAGTATCAGTGGT-3'
Ephrin-B2	sense	5'-GGGTATAGTACCAGGCCTTGTCC-3'	S1P1	sense	5'-TCCATGTAAACTGGGTCAAG-3'
	antisense	5'-GCTAGAAGCTGGTACAAATGGG-3'		antisense	5'-AAAGGTGCTGTAGGGGTTAG-3'
EphB4	sense	5'-CAGGTGGTCAGCGCTCTGGAC-3'	S1P3	sense	5'-ATGGCATTTGCTCTTGTTTA-3'
	antisense	5'-ATCTGCCACGGTGGTGAGTCC-3'		antisense	5'-TATTTTTCCCTTAACCCAGC-3'
Endoglin	sense	5'-GGTGTTCCTGGTCCTCGTTT-3'	PDGFRα	sense	5'-CAAACCCTGAGACCACAATG-3'
	antisense	5'-CAAAGGAGGTGACAATGCTGG-3'		antisense	5'-TCCCCCAACAGTAACCCAAC-3'
PDGFA	sense	5'-TGTAACACCAGCAGCGTCAAG-3'	PDGFRβ	sense	5'-TGCCTCAGCCAAATGTCACC-3'
	antisense	5'-CTGGACCTCTTTCAATTTTGGC-3'		antisense	5'-TGCTCACCACCTCGTATTCC-3'
GAPDH	sense	5'-TGATGGGTGTGAACCACGAG-3'			
	antisense	5'-GTCATTGAGAGCAATGCCAG-3'			

Table. S1. Reverse transcriptional PCR primer sequences are listed. Total RNA was isolated from LLC tumors grown in either $S1P_2^{+/+}$ or $S1P_2^{-/-}$ mice for 7-days using TRIZOL reagent. One microgram of total RNA was transcribed into first-strand cDNA using oligo(dT) 18 primer and ReverTraAce. One microgram of the reaction mix (out of 25 µl in total) was amplified by PCR conducted for 25-28 cycles transcribed DNA as template.
*, significance was detected between tumors grown in $S1P_2^{-/-}$ and wild.